NEW LOW ACCRETION-RATE MAGNETIC BINARY SYSTEMS AND THEIR SIGNIFICANCE FOR THE EVOLUTION OF CATACLYSMIC VARIABLES[1,2]

Gary D. Schmidt[3], Paula Szkody[4], Karen M. Vanlandingham[3], Scott F. Anderson[4], J. C. Barentine[5], Howard J. Brewington[5], Patrick B. Hall[6], Michael Harvanek[5], S. J. Kleinman[5], Jurek Krzesinski[5,6] Dan Long[5], Bruce Margon[8], Eric H. Neilsen, Jr.[9], Peter R. Newman[5], Atsuko Nitta[5], Donald P. Schneider[10],

AND

Stephanie A. Snedden[5]

gschmidt@as.arizona.edu
Accepted to the Astrophysical Journal, Part 1

ABSTRACT

Discoveries of two new white dwarf plus M star binaries with striking optical cyclotron emission features from the Sloan Digital Sky Survey (SDSS) brings to six the total number of X-ray faint, magnetic accretion binaries that accrete at rates $\dot{M} \lesssim 10^{-13}\ M_\odot\ \mathrm{yr}^{-1}$, or <1% of the values normally encountered in cataclysmic variables. This fact, coupled with donor stars that underfill their Roche lobes and very cool white dwarfs, brand the binaries as post common-envelope systems whose orbits have not yet decayed to the point of Roche-lobe contact. They are pre-magnetic CVs, or pre-Polars. The systems exhibit spin/orbit synchronism and apparently accrete by efficient capture of the stellar wind from the secondary star, a process that has been dubbed a "magnetic siphon". Because of this, period evolution of the binaries will occur solely by gravitational radiation, which is very slow for periods >3 hr. Optical surveys for the cyclotron harmonics appear to be the only means of discovery, so the space density of pre-Polars could rival that of Polars, and the binaries provide an important channel of progenitors (in addition to the asynchronous Intermediate Polars). Both physical and SDSS observational selection effects are identified that may help to explain the clumping of all six systems in a narrow range of magnetic field strength around 60 MG.

Subject headings: novae, cataclysmic variables — magnetic fields — polarization — stars: individual (SDSS J083751.00+383012.5, SDSS J132411.57+032050.5, SDSS J155331.12+551614.5, SDSS J204827.91+005008.9)

1. INTRODUCTION

The physics of radial accretion onto the surface of a white dwarf divides naturally into regimes defined by the specific accretion rate and local magnetic field strength (e.g., Lamb & Masters 1979; Wickramasinghe & Ferrario 2000 and references therein). For comparatively dense flows and weak fields, $\dot{m} \gtrsim 1\ \mathrm{g\ cm^{-2}\ s^{-1}}$, $B \lesssim 50$ MG, a strong shock radiates primarily by the bremsstrahlung mechanism (emissivity $\epsilon_{br} \propto N_e^2$) at a temperature common to both ions and electrons of $kT \sim 10 - 30$ keV. The highest accretion rates, $\dot{m} \gtrsim 100\ \mathrm{g\ cm^{-2}\ s^{-1}}$, are still cooled largely by hard X-rays, but the ram pressure of the stream can depress the shock below the level of the surrounding photosphere, so that the emergent reprocessed radiation appears predominately in the soft X-rays/EUV. More rarefied streams and/or stronger magnetic fields favor cyclotron emission ($\epsilon_{cyc} \propto N_e B^2$), which results in a reduced shock height and two-fluid plasma with the electrons being substantially cooler than the ions (Fischer & Beuermann 2001). At the typical total mass accretion rate of a magnetic cataclysmic variable (CV; $\dot{M} \sim 10^{-11} - 10^{-10}\ M_\odot\ \mathrm{yr^{-1}}$; e.g., Warner 1995), the conditions in the accretion region(s) are generally spanned by the above parameter range, and strong X-ray and polarized optical cyclotron emission are observed. In view of this fact, it is no coincidence that the current catalog of magnetic CVs (Ritter & Kolb 2003) is dominated by discoveries from orbiting X-ray observatories (especially *ROSAT*).

The recent initiation of large-area, deep optical surveys – generally targeted at the extragalactic universe – has un-

covered a sample of six accreting magnetic binaries that display remarkably prominent, detached, and circularly-polarized cyclotron emission harmonics atop the stellar continua (Reimers et al. 1999; Reimers & Hagen 2000; Szkody et al. 2003, hereafter S03). The almost complete lack of X-ray emission from these systems (Szkody et al. 2004; hereafter S04) explains how they eluded the earlier all-sky X-ray surveys and, together with the optical spectral appearance, implies an extremely low specific accretion rate, $\dot{m} \sim 0.001 - 0.01$ g cm^{-2} s^{-1}. Here, theory indicates that no shock forms (Kuijpers & Pringle 1982). This "bombardment" regime is a non-hydrodynamic solution that describes conditions in which the heated electrons cool on a time scale short compared with the stopping time of the protons (e.g., Woelk & Beuermann 1996 and references therein). In the case of a strongly magnetic white dwarf, the cooling occurs primarily by cyclotron emission at a low atmospheric column depth and at a temperature well below that of a radial shock ($kT \sim 1$ keV). Thus, virtually all of the accretion energy emerges in a few isolated emission features at low harmonic number. Though the very low-$\dot{m}$ regime was explored theoretically to explain observations of intense cyclotron lines in known AM Her systems during temporary episodes of low mass transfer (total accretion rate $\dot{M} \sim 10^{-12}$ $M_\odot$ yr^{-1}), it appears that the newly-discovered objects represent a distinct, possibly evolutionary, binary phase with even more extreme and persistent characteristics. Indeed, Schwope et al. (2002) have coined the term Low Accretion Rate Polar (LARP) to highlight their potential importance.

In this paper we report the discovery of two additional low-$\dot{m}$ magnetic binaries from recent Sloan Digital Sky Survey (SDSS) observations. Followup photometric, spectroscopic, and spectropolarimetric observations of these and previously-discovered examples are analyzed to gain insight into the currently small but intriguing class of objects. From this evidence we explore ideas as to their evolutionary state, space density, and relevance to both magnetic and nonmagnetic CVs. Preliminary discussion of these results was presented by Schmidt (2004), and some of the conclusions were reached by Webbink & Wickramasinghe (2004) from a more theoretical perspective.

2. OBSERVATIONAL DATA

The SDSS has proven to be an extremely valuable, if not optimized, tool for identifying various classes of stellar systems. More than 120 new CVs have been cataloged thus far (Szkody et al. 2005 and references therein), based on spectroscopy of targets selected by algorithms that are sensitive to regions of the color-color planes occupied by hot stars, QSOs, white dwarfs and white dwarf-M star pairs. Indeed, because of the presence of intense, narrow, cyclotron harmonics, three of the four SDSS low-$\dot{m}$ magnetic accretion binaries were targeted as candidate QSOs. The exception is SDSS J2048+0050[11], which exhibits comparatively weak features and was targeted as part of the Sloan Extension for Galactic Understanding and Evolution (SEGUE; e.g., Beers et al. 2004). As an illustration, we compare the locations of the four SDSS low-$\dot{m}$ systems

to other classes of objects in the SDSS $u - g$, $g - r$ plane in Figure 1.

The SDSS spectroscopic data are obtained with twin dual-beam spectrographs covering the regions $3900 - 6200$ Å and $5800 - 9200$ Å at a resolving power of $\lambda/d\lambda \sim 1800$. The wide, continuous spectral coverage provides broad sensitivity to cyclotron emission features, which may be prominent at only one or two harmonics of the cyclotron fundamental frequency $\omega_c = eB/m_e c$. Details of the SDSS photometric and spectroscopic hardware, as well as the data reduction procedures and targeting strategy, can be found in Fukugita et al. (1996), Gunn et al. (1998), Hogg et al. (2001), Lupton et al. (1999, 2001), York et al. (2000), Pier et al. (2003), Smith et al. (2002), and Ivezic et al. (2004).

Followup observations of known magnetic systems and confirmation of new candidates were made through optical spectroscopy and circular spectropolarimetry with the instrument SPOL (Schmidt et al. 1992) attached to the 6.5 m MMT atop Mt. Hopkins and the Steward Observatory 2.3 m Bok telescope on Kitt Peak. Polarimetric data are essential because of the $\sim$141 million objects imaged thus far by the SDSS, it is inevitable that there will be chance superpositions of QSOs and late-type Galactic stars whose total flux spectra mimic the binaries discussed here. As an example, SDSS J092853.51+570735.4 shows only marginal evidence for duplicity in the SDSS imaging, yet in the survey spectrum displayed in the bottom panel of Figure 2, exhibits a single emission feature at 4140Å and the molecular band structure of an M dwarf. In this respect it resembles the other two objects depicted in Figure 2. However, SDSS J0928+5707 shows no circular polarization to an upper limit of $v = V/I = 0.4\%$, and as also shown in the figure, subtraction of the spectrum of an M3 V spectrum reveals the blue continuum and emission lines of a $z = 1.67$ QSO. SDSS J164209.57+213352.8, with $z = 1.43$, and probably SDSS J155839.64+082720.1 and SDSS J105322.24+535510.1, are other cases that have been encountered thus far.

In the configuration used, the 1200×800 pixel SITe CCD used in the spectropolarimeter provides a coverage $\sim \lambda\lambda 4200 - 8400$ and resolution $\sim$15 Å. The thinned, back-illuminated, and anti-reflection coated device features broad sensitivity with quantum efficiency reaching 92% and a read noise of $2.3 e^-$. Circular spectropolarimetry is obtained from 4-exposure sequences in different orientations of a quarter-waveplate, with a Wollaston prism located in the collimated spectrograph beam splitting the light into the complementary senses of polarization required for measurement of a Stokes parameter. Total flux spectra are derived from the sum of the polarized spectra, with calibrations based on observations of spectral flux standard stars made in the identical instrument configuration on the same night, and terrestrial absorption features removed through observations of proximate early-type stars. Data reduction is carried out using custom *IRAF* scripts[12].

Two runs of CCD photometry were made on SDSS J0837+3830 on 2004 Nov. 30 and Dec. 1 in an effort

---

[11] For brevity, we will refer to objects in the text and figures by the designation SDSS J$hhmm\pm ddmm$.

[12] *IRAF* is distributed by the National Optical Astronomy Observatories, which are operated by the Association of Universities for Research in Astronomy, Inc., under cooperative agreement with the National Science Foundation.

to derive a photometric period. These observations were made in unfiltered light at the MDM 2.4 m telescope on Kitt Peak with the Templeton CCD (a 1024×1024 24μm pixel, thinned, back-illuminated SITe CCD). Seeing was poor, averaging $\sim$4″ FWHM on the first night and 6″ on the second, and the latter run was cut short by clouds. Integration times were 300 s throughout. The data frames were reduced using standard *IRAF* routines and field stars were used to perform the relative photometry.

Finally, time-resolved spectra, using 15 min integrations over the course of 4.3 hrs, were acquired for SDSS J2048+0050 on 2004 October 4 using the Apache Point Observatory (APO) 3.5 m telescope. The Double Imaging Spectrograph was used with the 1.5″ slit in high-resolution mode, resulting in a resolution of $\sim$3Å and wavelength coverage of $4000 - 5200$Å in the blue and $6000-7600$Å in the red. Reduction of the spectra to wavelength and flux was accomplished with standard *IRAF* routines using lamps and standard star frames obtained during the same night. Radial velocity and flux measurements of the Hα and Hβ lines were made with the "e" routine (which determines the line centroid) in the *IRAF* SPLOT package. A log of all of the above observations is provided as Table 1.

3. TWO NEW LOW ACCRETION-RATE MAGNETIC BINARIES

Two new binaries with prominent, isolated emission features have been identified from SDSS spectroscopy through the end of 2004. In coordinate and Plate-MJD-Fiber notation, they are: SDSS J083751.00+383012.5 = 828-52317-049, from Data Release 3 (DR3; Abazajian et al. 2005) and reported by Szkody et al. (2005), and SDSS J204827.91+005008.9 = 1909-53242-601. The latter object will be included in a future SDSS data release. Photometry is provided as SDSS *psf* magnitudes in Table 2.

In the SDSS spectra shown in Figure 2, distinguishing humps between 4000Å and 5000Å are evident in both objects, but basic differences between these spectra and those of previous low-$\dot{m}$ magnetic systems (Reimers & Hagen 1999; Reimers et al. 2000; S03) highlight the wide variety of the class: The hump in SDSS J0837+3830 dominates the underlying stellar continuum with a broad and rather flat-topped profile (FWHM $\gtrsim$ 1000Å), and it is accompanied by prominent narrow Balmer emission lines up to at least Hγ. Though the lines are likely more indicative of the conditions on the M-star surface than of any accretion stream, all of these characteristics are consistent with an accretion rate that may be slightly higher than has been estimated for the previous systems ($\dot{M} \sim 10^{-13}\ M_\odot$ yr^{-1}). In contrast, the single hump in SDSS J2048+0050 is weak compared with the cool companion, and even though a narrow Hα line is evident, Hβ is barely detected. If these features are characteristic of the binary over long time scales, the accretion rate would seem to be extremely low.

3.1. *SDSS J0837+3830*

Each of the two runs of CCD photometry on SDSS J0837+3830 shows a clear brightness variation on a timescale of a few hours. The two nights were therefore

---

[13] See also §4

combined and power spectrum analysis performed. The result displays two peaks of equal significance at periods of 3.18 and 3.65 hr, i.e., a difference of one cycle between the two nights. Least-squares fits to a sine wave yield a semi-amplitude of 0.06 mag in either case, and inspection suggests that the period with the slightly higher total χ^2, 3.18 hr, might actually be preferred because of fewer discrepant data points. This choice is depicted in Figure 3. Because the CCD was used unfiltered, it is not possible to categorically assign the photometric variation to a changing view of the magnetic field in the cyclotron emission region (the white dwarf spin period) as opposed to the varying aspect of a tidally-locked secondary star (the orbital period). However, where information is available for the previously-studied low-$\dot{m}$ systems listed in Table 3, indications are that spin-orbit synchronism has been established[13], and we presume that this is the case also in SDSS J0837+3830. Unfortunately, the interval between the photometric observations and our spectroscopy described below is too long to place the latter data on a phase scale.

All four epochs of followup spectroscopy of SDSS J0837+3830 yielded spectra that mimic the survey data shown in Figure 2: a single dominant cyclotron hump in the blue, narrow Balmer emission lines, and the continuum of a cool companion star with $R \sim 19.2$. Indeed, the observational record for this object is as extensive as for the previously-discovered low-$\dot{m}$ magnetic systems, and shows no evidence for high accretion states over a period of 3 yr. The longest run with the spectropolarimeter spanned slightly more than 1.2 hr, or $\sim$40% of the photometric period, while the object was setting on the evening of 2004 May 13. As depicted in Figure 4, each of the five 800 s sequences displayed circular polarization of nearly -20% in the 4500Å hump, and a second negatively-polarized feature is present near 6200Å. For a low plasma temperature, these can be readily assigned to harmonics $n = \omega/\omega_c = 4$ and 3, respectively, in a field of 65 MG. However, the shape of the $n = 3$ circular polarization harmonic is distorted into a peaked profile, and significant *positive* circular polarization, $v = 2 - 4$%, is measured between the harmonics. This indicates that the oppositely-polarized magnetic pole is also accreting, and that it may have a slightly different field strength as well as a lower accretion rate. Variations through the sequence are confined to a reduction in the emission-line strength and possible fading of the $n = 4$ harmonic. The constancy in radial velocity of the Hα emission line to $\leq$50 km s^{-1} and the small amplitudes of polarimetric and photometric variability suggest that this binary may be oriented at a low inclination.

3.2. *SDSS J2048+0050*

The APO spectra of SDSS J2048+0050 appear very similar to the SDSS spectrum shown in Figure 2, which was obtained about 1.5 months earlier. The blue spectra cover the cyclotron hump near 4550Å and Hβ, while the red spectra follow Hα and the TiO bands. The Balmer lines are very narrow, ruling out an origin in an infalling stream, and He II λ4686 is not present, indicating the lack of a hard

irradiating continuum. The time-resolved spectra show a changing amplitude of the cyclotron hump and strength of the Balmer emission, with the Hβ line disappearing completely in several spectra. Least squares fitting of the velocity measurements to a sinusoid yields a period of 4.2 hr (250 min) for Hα with a K semi-amplitude of 153 ± 5 km s^{-1} and rms deviation of 14 km s^{-1} around the fit. Hβ was more difficult to measure and had fewer samples due to its disappearance at some phases, so the period was fixed at 250 min to derive a best fit solution with $K = 124 \pm 7$ km s^{-1} and an rms of 18 km s^{-1}. Again, our knowledge of the period is insufficient to link to other datasets. The fits are shown along with the data points and Hα line fluxes in Figure 5. A least-squares sine fit to the fluxes indicates that the peak flux is offset by ~ 0.14 phase from the negative-to-positive velocity zero-crossing that defines $\varphi = 0$. The implications of these observations are that the lines originate predominately from the inner hemisphere of the secondary star, similar to the conclusion reached for WX LMi (HS 1023+3900) by Schwope et al. (2002), but the emission is not symmetric around the line of centers. If the enhanced emission is caused by irradiation of the secondary by a hot area near the accreting pole of the white dwarf, then it is likely that the pole is not directly opposite the secondary. Among the spin-orbit synchronized magnetic CVs (Polars) it is common to find the principal magnetic pole advanced somewhat prograde of the secondary in its orbit (Cropper 1988).

Spectropolarimetry of SDSS J2048+0050 has thus far been limited to slightly more than 1 hr obtained through cirrus on the 2.3 m telescope. The data were acquired in five sequences, and very little variation can be detected through the series. The combined flux spectrum, shown in Figure 6, again closely resembles the SDSS spectrum in Figure 2 both in absolute brightness and in the presence of a single hump centered near 4550Å. Hα is weak and Hβ is absent altogether at this combination of S/N and resolution. The net circular polarization in the 4550Å feature is extremely high at -38%. This, coupled with the fact that the peak flux of the feature is elevated only $\sim 40\%$ above the stellar continuum, implies that the cyclotron light in this harmonic must be essentially 100% circularly polarized! The polarization also dips slightly below zero around 6200Å, suggesting the presence of a second, weaker cyclotron harmonic akin to that in SDSS J0837+3830. If real (see §5), the harmonics have the same numerical assignment as in that system and the magnetic field strength is very similar at ~ 62 MG. No evidence exists for emission from the opposite magnetic pole, at least during the phase interval recorded by the spectropolarimetry.

SDSS J2048+0050 may be associated with a weak X-ray source in the $ROSAT$ All Sky Survey (RASS) at the level of 0.014 count s^{-1}, although there are other optical objects within the error circle. Using the crude conversion of 1 count s$^{-1} = 7 \times 10^{-12}$ erg cm^{-2} s^{-1} and a distance of 260 pc (derived below), a $0.1 - 2.4$ keV X-ray luminosity of $L_X \sim 8 \times 10^{29}$ erg s^{-1} is found. This would be approximately an order of magnitude larger than the measurements of L_X for SDSS J1553+5516 and SDSS J1324+0320 by S04, which were interpreted to arise from coronal emission on the secondaries. The result for SDSS J2048+0050

is extremely uncertain and begs for a deeper observation.

4. NEW RESULTS ON KNOWN LOW-$\dot{m}$ SYSTEMS

4.1. *Orbital Variations in SDSS J1324+0320*

The cyclotron emission harmonics in SDSS J1324+0320 display the greatest contrast relative to the underlying continuum of any of the low-$\dot{m}$ systems discovered thus far. The SDSS spectrum was presented by S03 together with a single observation of confirming spectropolarimetry, and a magnetic field strength of 63 MG was estimated from the identification of the humps with harmonics $n = 2$ (8200Å), 3 (5600Å), and 4 (4600Å). A period of ~ 2.6 hr was also derived from a 1.3 mag modulation in the r-band light curve. Because the cyclotron features overwhelm the stellar components in the optical, this period was ascribed to the rotation of the white dwarf, which was presumed to be synchronized to the orbital motion. The system was undetected in the RASS and produced only 0.0012 ± 0.0003 count s^{-1} in the most sensitive XMM-Newton detector (the EPIC pn; S04).

A full orbit of circular spectropolarimetry of SDSS J1324+0320 obtained at the MMT in 2004 Feb. is presented in Figure 7. The time sequences represent the circularly polarized spectral flux[14], $-v \times F_\lambda$, and total flux, F_λ, for successive 13 min observations. Prior to display, the spectrum of an M6 V star was subtracted from the data, as this spectral type was determined by S03 to best match the band features. It is clear from inspection that the dominant $n = 3$ harmonic at 5600Å is indeed the origin of the dramatic modulation in the r-band light curve, but plasma effects cause an even greater variation in the circularly polarized flux. In the first and last few observations of the series an extremely weak, narrow Hα emission line can be recognized in the total flux spectrum. The integrated flux and radial velocity of this feature have been measured for all spectra in which it can be discerned, and the results are shown in Figure 8. The accompanying least-squares sinusoidal fits to the variations show that the minimum in Hα flux nearly coincides with the positive zero-crossing of radial velocity (uncertainties in times of zero-crossing for the fitted curves are each slightly more than 0.1 hr). As in SDSS J2048+0050, we assign $\varphi = 0$ (UT ≈ 10.6) to this crossing. Combined with a velocity semi-amplitude of 342 ± 146 km s^{-1}, the characteristics argue for a system viewed at a high inclination, with the line emission confined largely to the inner hemisphere of the companion. $\varphi = 0$ then corresponds to the time that the secondary star and white dwarf are most nearly aligned along our line of sight. The antiphasing between Hα line strength and overall cyclotron flux in Figure 7 additionally implies that the dominant accreting pole of SDSS J1324+0320 is located on the inner hemisphere of the white dwarf. As is true for the other low-$\dot{m}$ systems, the agreement between the 2.6 hr photometric period and the independently derived spectroscopic value of 2.62 ± 0.24 hr implies that the white dwarf spin and binary motion are locked.

The spectral sequences in Figure 7 offer an instructive display of the emission properties of a magnetized plasma. The cyclotron absorption coefficient at low temperatures is such a steep function of frequency in the first few harmon-

---

[14] Note that the polarized flux has been negated to facilitate comparison with the total flux spectra.

ics, $\alpha \propto (\omega_c/\omega)^{10-12}$ (e.g., Meggitt & Wickramasinghe 1982; Chanmugam et al. 1989), that the observed characteristics can vary markedly from one harmonic to the next. As an example, the flux ratio of harmonic $n = 3$ to harmonic 2, $F_3/F_2 > 1$, signifies moderately high optical depth in these features, since it would saturate at the Rayleigh-Jeans ratio $(\omega_3/\omega_2)^3 \approx 3.4$ for $\tau \to \infty$. At the same time, the comparative weakness of the 4600Å harmonic, $F_4/F_3 < 1$, implies that the plasma suddenly becomes optically thin at $n = 4$. It is the combination of the steep harmonic dependence of opacity, low temperature, and modest column depth that accounts for the cyclotron emission in these systems being so narrowly confined to just the few lowest harmonics.

A rather high optical depth at $n = 2$ is also indicated by the modest polarization of this harmonic, $\lesssim 10\%$, as compared with $v = 50 - 70\%$ reached in harmonic 4. The angular sensitivity of the cyclotron opacity means that, in the absence of dilution, the smallest optical depth and therefore largest circular polarization for reasonably thick features like the $n = 2$ and 3 features will occur for vantage points that approach the magnetic field axis. From the data of Figure 7, this evidently occurs near $\varphi = 0$ (10.6 UT). The fact that both the total and polarized flux at $n = 4$ are actually reduced at this phase attests to this feature being optically thin throughout.

Beyond this qualitative understanding, the situation becomes more complex. Ferrario et al. (2004) encountered difficulties in modeling the detailed behavior of the harmonics in SDSS J1553+5516 and SDSS J1324+0320 when they noted that the fluxes in harmonics 2 and 3 in Figure 8 are actually *lowest* at phases where the optical depth as indicated by the degree of polarization is *largest*. This is contrary to predictions of the standard model. Ferrario et al. obtained some success with a model that recognizes the effects of ram pressure in compressing the upper white dwarf atmosphere. The significance of this fact is that cyclotron emission from the impact region would then traverse and be attenuated by cooler regions of the surrounding undisturbed photosphere for a certain range in viewing angle. Faraday mixing and depolarization might also be important, and for this reason phase-dependent linear spectropolarimetry of one of these systems would be valuable.

4.2. *Orbital Variations in SDSS J1553+5516*

Coarse phase-resolved spectroscopy and a single spectropolarimetric observation of SDSS J1553+5516 were presented by S03 and point-source models of phase-resolved spectropolarimetry were discussed by Ferrario at the 2002 Capetown IAU colloquium (190) on magnetic cataclysmic variables (unpublished). Summarizing those conclusions with respect to the new time series data obtained on 2002 May 8 and shown in Figure 9, cyclotron emission is arising in a relatively cool plasma, $kT \sim 1$ keV, that is moderately optically thick at the $n = 3$ (6200Å) harmonic, but optically thin at all phases at $n = 4$ (4650Å). Indeed, defining orbital phase $\varphi = 0$ by the positive zero crossing of emission line radial velocity at 7.9 UT (see below), the Doppler effect alone would broaden features beyond the narrow structure that is observed in polarized flux ($v \times F$) near $\varphi = 0.75$ and 0.25 (6.5 and 9.0 UT, respectively)

unless $kT \lesssim 1$ keV. The horn-shaped appearance of the $n = 3$ harmonic in polarized flux evident over a broad interval around $\varphi = 0$ (7.3 − 8.6 UT) is even more prominent in fractional circular polarization, $v(\%)$. This is characteristic of a plasma with modest optical depth, where the intensity at the harmonic peak approaches the blackbody limit in the extraordinary ray (Rousseau et al. 1996; Ferrario et al. 2004).

Because of its relative brightness, the Hα emission line in SDSS J1553+5516 is rather easily measured, and analysis of the data of Figure 9 yields the radial velocity curve depicted in Figure 10. The phasing and amplitude ($K = 250 \pm 18$ km s^{-1}) of the line, shown by filled circles, is shared by the λ7050 TiO bandhead (crosses), conclusively showing that both arise on the secondary star. The fact that the photometric period of 4.39 hr reported by S03 also matches the spectroscopic variations proves the existence of spin-orbit synchronism. Finally, we point out that the maximum in Hα emission-line flux occurs near the end of the sequence in Figure 9 ($\varphi \sim 0.5$), once again indicating that the chromospheric emission is concentrated on the inner hemisphere of the companion.

5. SECONDARY STARS AND DISTANCES

The secondary stars that are so evident in low-$\dot{m}$ systems currently provide our only indicators of distance. From a comparison of the observed molecular band spectra to those of main sequence stars, Reimers & Hagen (1999) and Reimers et al. (2000) estimated spectral types of M3.5 and M4.5 for the companions in HS 0922+1333 and WX LMi, respectively, and the observed spectral fluxes relative to late-type spectral standards with parallax measurements, lead to distance estimates of ∼140 and 190 pc. These values and the quoted total mass accretion rates are listed in Table 3, though it is useful to point out the uncertainties in this technique, as Schwarz et al. (2001) find a somewhat smaller value ($D \sim 100$ pc) for HS 0922+1333.

In applying the same method to the SDSS examples, it appeared that the lack of readily available, accurately flux-calibrated optical spectra of M dwarf standards was a significant difficulty, so the calibration observations described in the Appendix were undertaken. Those results provide easily computed absolute monochromatic fluxes in several narrow spectral bands over the range 4700 − 7500Å for M dwarfs from M0 to M6.5. The relations presented therein were used in the following analysis.

Spectral types for the secondaries of SDSS J1553+5516 and SDSS J1324+0320 were judged by S03 to be M5 and M6, respectively, and we adopt their classifications. For SDSS 0837+3830 and SDSS 2048+0050, the spectra in Figure 2 offer good S/N and wide spectral coverage, and comparison of these to the SDSS M dwarf standards from Hawley et al. (2002) leads to estimates of M5 and M3, respectively (it is our opinion that uncertainties in the process do not warrant the claim of fractional subtypes). Using these spectral types, best cancellation of the molecular features was found for secondary fractions in the 7450 − 7500Å calibration band of 80%, 45%, 60%, and 90% for the stars SDSS J1553, 1324, 0837, and 2048, respectively. The resulting spectra are presented in Figure 11. The use of eq. A1 together with the coefficients in Table A1 then yield the distances and mass accretion rates listed

in Table 3. For reference, an accretion rate of 10^{-13} $M_\odot$ yr^{-1} corresponds to a luminosity $L_{acc} \sim 6 \times 10^{29}$ erg s^{-1}. The distance estimate to SDSS J1553+5516 is somewhat larger than the 100 pc used by S03, but the values are probably consistent to within the accuracy of the technique. In fact, considering the combined uncertainties in spectral classification of the secondaries, fractional contributions to the spectra, standard calibration, and slit/fiber losses, distances to individual objects should not be trusted to better than 50%, or the resulting luminosities to a factor of two. Note that the spectrum of SDSS J2048+0050 displayed in Figure 11 exhibits a broad bump around 6600Å that exceeds the residuals from the M-star subtraction and that we take in support of our polarimetric identification of the $n = 3$ cyclotron harmonic (§3.2).

In computing the total mass accretion rates, the white dwarf mass was taken to be 0.6 $M_\odot$ and gravitational energy was assumed to be converted solely into cyclotron flux (see, however, §6), with only a small allowance for harmonics outside the observed window. The flux progression in the observed harmonics, which typically peaks at $n = 3$, supports this view. The exception is SDSS 0837+3830, which apparently is not optically thin in the bluest harmonic measured ($n = 4$). For this system the uncertainty in $\dot{M}$ is somewhat higher. The absence of significant X-ray emission has been demonstrated for SDSS J1553+5516 and SDSS J1324+0320 (S04), and theory (e.g., Woelk & Beuermann 1992) asserts that this should be the case for the field strengths and specific accretion rates indicated by the cyclotron spectra.

6. PRIMARY STAR TEMPERATURES

Temperatures for the white dwarfs have been estimated at $T_{\rm eff} \leq 10,000$ K for both HS 0922+1333 and SDSS J1553+5516 (Reimers et al. 1999; S03), and 13,000 K $\pm$ 1000 K for WX LMi (Reimers & Hagen 2000). All are unusually cool in comparison to the primaries of Polars, which themselves are cooler than the white dwarfs in nonmagnetic CVs (Sion 1999). The difference between the latter two classes is understood to reflect different levels of accretion-induced heating, largely compressional heating of the interior (Townsley & Bildsten 2002). By extension, the temperature limit for SDSS J1553+5516 not only implies that the system is relatively old, $\tau_{cool} \gtrsim 0.7$ Gyr, but can be used to constrain the mean accretion rate over the past $\sim 10^6$ yr to $\langle \dot{M} \rangle \lesssim 3 \times 10^{-12}$ $M_\odot$ yr^{-1} (Townsley & Bildsten 2004; S04).

Analysis of the spectra of the other three SDSS systems yields similarly low estimates: $T_{\rm eff} \lesssim 14,000$ K for SDSS J0837+3830 and $\lesssim 7,500$ K for both SDSS J1324+0320 and SDSS J2048+0050. Each of these values is based on the observed flux level in a gap between cyclotron harmonics, after subtraction of the best-fitting M dwarf template, and makes use of surface fluxes from the nonmagnetic $\log g = 8$ DA model atmospheres summarized by Bergeron et al. (1995). We have also assumed a stellar radius of 8×10^8 cm (appropriate for $M_{wd} \sim 0.6$ $M_\odot$), and include an allowance of 50% above the distances listed in Table 3 to account for the uncertainties in those estimates. While higher mass white dwarfs (smaller radii) would permit higher temperatures, values increase by only $20 - 50\%$ for $M_{wd} = 1$ $M_\odot$, and in any

case the possibility of additional emission sources contaminating the gaps renders the estimates upper limits.

In evaluating the spectra, it was evident that the spectral shape of the underlying continuum occasionally appeared hotter than the temperature indicated by the measured flux at a specific wavelength. The situation is depicted in Figure 11 as a comparison between the secondary-subtracted SDSS spectra and model stellar energy distributions. Because the model temperatures, which range from 5,500 K for SDSS J1324+0320 to 9,500 K for SDSS J0837+3830, were computed on the basis of the flux at a cyclotron-free wavelength in the interval $5000 - 5600$Å, the continua match here. However, for SDSS J1553+5516 and SDSS J2048+0050 the model atmospheres fall well short of the measured flux around 4000Å. The spectrum of SDSS J1324+0320 is too faint in the blue for a reliable comparison and the broader $n = 4$ harmonic in SDSS J0837+3830 confounds the assignment of the stellar continuum at the shortest wavelengths.

The inconsistency between continuum shape and absolute flux level for at least SDSS J1553+5516 and SDSS J2048+0050 is reminiscent of the difficulties that plague temperature determination of non-accreting highly magnetic white dwarfs, where observed optical continua are found to be significantly steeper than predicted by non-magnetic white dwarf models (e.g., Schmidt et al. 1986; Gänsicke et al. 2001). However, the disparity is considerably greater in the low-$\dot{m}$ systems, despite a field strength ($\sim$65 MG) below the level at which substantial effects on the emitted continuum are expected ($>$100 MG). Unfortunately, the best attempts to estimate bound-free opacities in the presence of a strong magnetic field (Merani et al. 1995) have not proven to be noticeably better in explaining the observed spectral energy and polarization distributions (Jordan & Merani 1995) at high strengths.

We suggest that a more viable explanation of the differences between indicators of stellar temperature is the presence of a heated cap surrounding the magnetic pole(s). Irradiated hot spots are known to be important in and around the impact regions of Polars, where temperatures as high as 3×10^5 K and sizes up to a fraction $f = 0.1$ of the stellar surface are measured (e.g., Vennes et al. 1995; Gänsicke et al. 1998; Mauche 1999). Even if cyclotron emission is the dominant cooling mechanism in a low-$\dot{m}$ system, approximately half of that radiation will be directed downward, where it will be intercepted and reradiated in the UV or EUV by the white dwarf photosphere. Considering the sizes of the impact regions on Polars, a hot spot covering $2 - 5\%$ of the stellar surface in a low-$\dot{m}$ magnetic binary would not be unreasonable. From simple simulations using blackbodies (Gänsicke et al. 1998; Mauche 1999) we have found that a spot with $T_{\rm eff} = 20,000$ K and $f = 0.04$ could steepen the net continuum of a star with a surface temperature of 8,500 K to an equivalent temperature of $>$10,000 K, while increasing the absolute flux in the optical by only $\sim$30%. Other combinations are, of course, possible.

The total luminosity of a hot spot with the above characteristics implies a total accretion rate $\dot{M} \sim 4 \times 10^{-13}$ $M_\odot$ yr^{-1}, slightly higher than the highest rates indicated by the optical cyclotron luminosity in Table 3. However, there is independent evidence in favor of such spots in the form

of the flux-modulated narrow Balmer emission lines described in §3 and 4. While Balmer emission is a common attribute of active late-type stars, in each of the four SDSS examples the line flux was found to be enhanced on the inner (irradiated) side of the secondary. Assuming that each ionizing photon incident on the secondary gives rise to one Hα photon, a spot with $T_{\rm eff} = 20,000$, $f = 0.04$ could account for a luminosity $L_{\rm H\alpha} \sim 3 \times 10^{26}$ erg s^{-1} in a binary with $P = 4$ hr. This is a significant fraction of the $2 - 20 \times 10^{26}$ erg s^{-1} measured in the modulated portions of the line. Higher temperatures and lower covering factors would bring the numbers into better agreement. The fact that SDSS J0837+3830 exhibits the largest measured Hα luminosity, as well as the highest inferred accretion rate and hottest white dwarf of the SDSS objects, is a reassuring consistency check. Some support is also provided by the (marginal) detection of a ~46 eV component in the EUV portion of the *XMM-Newton* spectrum of SDSS J1553+5516 (S04) that could not be explained by coronal emission from the secondary star. A more definitive test is possible in the form of UV/EUVE photometry through an orbital cycle (à la Gänsicke et al. 1998), indeed NUV/FUV observations of SDSS J1553+5516 are in the queue for *GALEX*. If irradiated accretion spots contribute significantly to the optical continua of the low-$\dot{m}$ magnetic binaries, the implication is that the physics of the impact region involve more cooling mechanisms than have been discussed to date.

7. LOW ACCRETION-RATE MAGNETIC SYSTEMS AS PRE-POLARS

7.1. *Undersized Companions*

The total accretion rate estimates in Table 3, $\sim 5 \times 10^{-14} - 3 \times 10^{-13}$ $M_\odot$ yr^{-1}, are all <1% of the values typically measured for Polars during high accretion states. In fact, the numbers bear more similarity to the integrated solar wind mass loss rate of 2×10^{-14} $M_\odot$ yr^{-1}. The tendency of diskless CVs to lapse into periods of inactivity is well known, but even in low states the accretion luminosities of Polars are nearly an order of magnitude larger than we have measured for the low-$\dot{m}$ systems (Ramsay et al. 2004). Furthermore, the durations of Polar low states are typically found to lie in the range of weeks to ~1 yr[15], and the overall duty-cycle of accretion appears to be ~50% (Hessman et al. 2000; Ramsay et al. 2004). In contrast, none of the objects listed in Table 3 has ever been observed in a high state, despite repeated telescopic visits separated by intervals as long as a few yr (Table 1 and Schwarz et al. 2001). These facts, coupled with the low surface temperatures found for the primary stars, motivate their identity as a new class of chronically low-$\dot{m}$ systems.

An explanation for the distinctively low accretion rates and a clue to their evolutionary status is the fact that in all six cases the secondary stars appear to underfill their Roche lobes. This has already been noted for WX LMi by Schwarz et al. (2001), who pointed out that a star with the measured spectral type of M4.5 V has a radius 20% smaller than the Roche lobe for $P = 2.8$ hr. The lobe dimensions scale directly with stellar separation, therefore

the overall situation can be appreciated simply by noting that the spectral type expected for a Roche lobe-filling main-sequence star varies from M2 at a period of 4 hr to M4.5 at $P = 2$ hr. These types are systematically earlier (by 0.5 to 3 subtypes) than the measured spectral types in Table 3. Moreover, the mean difference of nearly 1.5 subtypes is large enough to accommodate any modern mass-radius relation for the lower main sequence as well as primary star masses as large as the Chandrasekhar limit. Beuermann et al. (1998) and Baraffe & Kolb (2000) have pointed out that, among CVs in general, a spectral type difference in the same sense is observed for systems with $P > 3$ hr. Simulations by Baraffe & Kolb indicate that the general trend observed for $3 < P < 6$ hr, as well as the width of the $2 - 3$ hr period gap, can be explained by the donor stars being out of thermal equilibrium owing to mass loss at a rate $\dot{M} = 1 - 2 \times 10^{-9}$ $M_\odot$ yr^{-1}. While this accretion rate is in rough agreement with what is inferred from luminosity estimates for disk CVs above the gap, the generally much lower luminosities of Polars have long been interpreted to imply that they accrete at rates $1 - 2$ orders of magnitude less, a fact explicable by the inhibiting effects of the primary star's magnetic field on magnetic braking from the donor (Webbink & Wickramasinghe 2002 and references therein). Thus, in the Baraffe & Kolb (2000) scenario, the systematic difference in spectral type should not exist for secondary stars in the synchronized magnetic CVs. Unfortunately, Polars are strongly clustered below the period gap, and only 4 systems exist with $P > 3$ hr in the list analyzed in the above studies. Among them is V1309 Ori at $P = 8$ hr, whose M0.5 secondary is evolved (Garnavich et al. 1994). There is a hint that companions in the remaining 3 magnetic objects are $0.5 - 1$ subtype later than expected for main sequence donors, but a larger sample is required to confirm or reject the notion.

Questions about the secondaries in Polars notwithstanding, mass loss rates of $<10^{-12}$ $M_\odot$ yr^{-1} imply evolutionary timescales far longer than the donor star's thermal timescale. For the same accretion rates, irradiation of the secondary star amounts to at most a few percent of its normal photospheric output, even for the shortest orbital periods. Thus, there is every reason to assume that the secondaries in low-$\dot{m}$ systems have the properties of main-sequence stars.

7.2. *A "Magnetic Siphon" of the Stellar Wind*

The diminutive sizes of the companions in low-$\dot{m}$ systems coupled with evidence that the binaries have been in protracted states of very weak accretion strongly suggest that some or all of the systems have never achieved Roche-lobe contact - i.e., that they are *pre*-Polars. The absence of detached magnetic white dwarf + M star binaries has been a subject of recent discussion (Silvestri et al. 2005; Liebert et al. 2005), with the realization that selection effects must be playing a significant role. Identifying the low-$\dot{m}$ magnetic binaries as the immediate precursors of at least some Polars would solve part of the riddle, leaving open the question of the whereabouts of long-period systems that never experience the common-envelope phase of

---

[15] The glaring exception is the ultrashort period system EF Eri, which has been in a protracted low state since 1997 (Wheatley & Ramsay 1998) but this binary more appropriately belongs near the opposite end of the evolutionary spectrum from the systems discussed here (Harrison et al. 2004).

evolution. In this picture, LARPs, while most definitely "Polar"ized, are not CVs at all, but pre-CVs.

In a binary that has not yet evolved to the point of Roche-lobe overflow, some portion of the secondary star's stellar wind will always arrive at the surface of the white dwarf[16]. For nonmagnetic primaries, the accreted fraction is very small, and the gravitational energy is an insignificant heating source spread over a large fraction of the white dwarf surface. However, a strongly magnetic primary couples effectively to the magnetic field lines of the secondary (Li et al. 1994), so plasma that would otherwise be centrifugally driven to large distances ends up on the white dwarf. Moreover, Li et al. find that, above a critical magnetic field strength, this "magnetic siphon"[17] is capable of collecting the *entire* stellar wind from the secondary. Webbink & Wickramasinghe (2004) offer an analytic argument based on energy densities that arrives at the same conclusion. The critical field strength depends on orbital period and geometry (Li et al. 1995), but appears to be in the range $50 - 100$ MG. Thus, at $B \sim 60$ MG, it is quite possible that the low-$\dot{m}$ systems discussed here represent examples where the magnetic siphon is essentially perfect. Ironically, the effects of the magnetic field are essential both in capturing the wind and in confining the resulting emission to a few very prominent features in the optical. If either process were not active, the objects would not stand out in optical AGN surveys, and thus would not be isolated for study. Selection effects in the SDSS are discussed at more length below.

It is important to note that, while stellar chromospheric/coronal activity and rotational spin-down are intensely studied effects of mass loss from late-type stars, thus far only upper limits ($\lesssim 10^{-10} M_\odot$ yr^{-1}) have been established for the actual wind rates (e.g., Wargelin & Drake 2001). The mass accretion rates inferred for low-$\dot{m}$ magnetic accretion binaries may therefore prove to be the first true measures of the amount of material carried away. To apply the results to single stars, corrections will have to be made for the facts that the binary examples present a reduced gravitational barrier and are in forced rapid rotation, but even these adjustments will be unnecessary for evaluating recent suggestions that the long-held magnetic braking model for CV evolution may be much less effective than previously thought (cf. Pinsonneault et al. 2002; Kolb 2002).

7.3. *Thoughts on Evolution*

The low-$\dot{m}$ systems offer interesting insight into the possible evolutionary stages of a magnetic binary. We make the standard assumption that a pre-CV emerges from the common envelope (CE) detached and with the degenerate core in asynchronous rotation. Whether the orbital period of a post-CE binary is affected by the presence of a magnetic field on the degenerate core is a matter of some debate (Liebert et al. 2005). However, assuming that tidal forces on the secondary are sufficiently strong, the binary orbit will decay and the period decrease under the relatively vigorous effects of magnetic braking via the secondary star's entrained wind (e.g., Verbunt & Zwaan 1981). The next major event - synchronization of the

white dwarf spin and orbital periods, or the initiation of accretion by Roche-lobe overflow - depends on the primary star magnetic field strength and secondary size: a modest magnetic field paired with a comparatively massive secondary will initiate Roche-lobe overflow first and appear at relatively long periods as an Intermediate Polar or other disk CV not yet recognized to be magnetic. In this case, a magnetic interaction between the stars may eventually synchronize the system at a shorter period and a Polar will ensue. If, however, the field strength on the white dwarf is high and/or the secondary star small, the locked status of the pre-Polars tells us that synchronization can occur *prior* to the onset of Roche-lobe overflow, at a period of at least 4.4 hr for $B = 60$ MG. As the white dwarf spin and orbital periods approach a common value, and while the stellar wind can still couple to open field lines of the white dwarf, spin-down might be assisted by the cooperative magnetic braking mechanism originally suggested by Schmidt et al. (1986) but shown to be ineffective once a synchronized state is achieved (Li et al. 1994).

It is difficult to imagine a magnetic siphon operating efficiently in a binary whose spin and orbital motions are uncoupled. Therefore, we take the onset of synchronism to be accompanied by the disappearance of angular momentum loss by magnetic braking. The estimate of Webbink & Wickramasinghe (2004) that this might occur in binaries as large as $a \sim 10 R_\odot$ is probably optimistic, but it suggests the potential effectiveness of the process. The pre-Polar now enters a possibly protracted era of period evolution governed solely by gravitational radiation and accreting by a magnetic siphon effect on the stellar wind. Interestingly, nova eruptions may actually occur during this phase, but the recurrence time would be exceedingly long (~ 1 Gyr). Eventually, Roche-lobe contact is established in this already synchronized binary, and a Polar is formed. Our estimate of $T_{\rm eff} \leq 5,500$ K of SDSS J1324+0320 at $P = 2.6$ hr demonstrates that the total time elapsed between the common envelope and Polar states can exceed 4 Gyr. This, together with the existence of an Intermediate Polar stage for other systems, offers a ready explanation for the propensity of Polars to exist at short orbital periods.

8. DISCOVERY AND CENSUS OF PRE-POLARS

The identification of 4 pre-Polars in the first ~ 5000 deg^2 surveyed by the SDSS suggests that an additional $1-2$ will be found before completion of the project and that ~ 30 would be cataloged if the entire sky were surveyed. From Table 3, the effective sampling distance of such a survey might be estimated at $D \sim 300$ pc, i.e., similar to the volume surveyed for X-ray bright (Polar) systems by *ROSAT* (Beuermann & Burwitz 1995), which discovered $\sim 80\%$ of the 80 known Polars. Thus, at face value, the space density of systems in the pre-Polar state might be expected to be about half of that for currently accreting Polars. The ratio is similar to that implied by a comparison between 4 pre-Polars and the 14 confirmed Polars that have been found in the portion of the sky sampled through SDSS DR4 (Szkody et al. 2005 and references therein).

---

[16] This is the same stellar wind that is held accountable for the dominant angular momentum loss in long-period disk CVs.

[17] An apropos term coined by R. Webbink.

However, questions of completeness must be raised. First, from the discussion in §7, the detectability of pre-Polars is expected to decline rapidly with increasing orbital period. If magnetic energy density is the key criterion (e.g., Webbink & Wickramasinghe 2004), the r^{-3} decline in field strength of a dipole implies that the effectiveness of the magnetic siphon will scale as $\sim P^{-4}$. At the other extreme, the probability of the secondary in a pre-Polar contacting its Roche surface increases as the period decreases, meaning that only pre-Polars with tiny secondaries (like SDSS J1324+0320) will be found at very short periods, and those will be produced only after long episodes of slow evolution. The magnetic field on the white dwarf is also an important variable, since the weaker-field systems will tend to reach Roche contact prior to synchronizing, and an Intermediate Polar *vs.* pre-Polar will characterize the phase leading up to the synchronized state.

Second, selection effects within the surveys can be important. The SDSS is aimed at being complete only for QSOs and galaxies (Stoughton et al. 2002). One fiber per spectroscopic plug-plate is dedicated to CVs and in practice samples objects in the white dwarf + pair region of the color-color planes. Another category for standards is a source of hot white dwarfs. Nevertheless, objects that fall in the QSO locus have the highest probability of being targeted because of the much larger number of fibers available. In order to estimate the effects of these constraints on the completeness of a putative population of pre-Polars, we have computed the SDSS colors of a synthetic spectrum consisting of a white dwarf, M star, and cyclotron emission for field strengths ranging from $0-200$ MG. The measured spectra of SDSS J1553+5516 and SDSS J1324+0320 were used to form a cyclotron template with realistic harmonic intensities and intensity ratios, but the spacing and width (in Å) of the harmonics were varied according to the assumed field. Broadband colors in the SDSS system were then computed and run through the (complex) SDSS QSO targeting algorithm (Richards et al. 2002) to determine which regimes in field strength would be most likely to result in objects selected for fiber spectroscopy and lead to recognition as pre-Polars.

As an example, we have overplotted the results of our simulation in the $u - g$, $g - r$ plane in Figure 1, with points separated by equal intervals in $\log B$ and fiducial field strengths (in MG) indicated by numbers adjacent to the track. Remember that there are 3 other color-color planes involved in the targeting decisions not shown here. At comparatively weak magnetic fields, all of the low-n cyclotron harmonics lie in the IR and the object is rejected from spectroscopic targeting by the QSO algorithm as the white dwarf + M star pair that it is. At $B = 30$ MG, the $n = 4$ harmonic enters the z photometric band and the object is briefly targeted as a high-z QSO. However, from our previous discussion on the sensitivity to field strength, such a system might not achieve a synchronized/siphoned state as a detached binary. As B continues to increase, the object approaches the stellar locus and loses targeting until the QSO algorithm is once again triggered for virtually the entire interval $50 < B < 90$ MG. This is the region in which all four SDSS pre-Polars have been found. For $90 < B \lesssim 200$ MG, brief intervals exist where the binary again receives high- or low-z QSO targeting, but for the

most part it is rejected due to the proximity of the track to white dwarfs and other excluded classes of stars. Above $B \sim 400$ MG (should such systems exist), the cyclotron fundamental shifts shortward of the u photometric band, and the object returns to obscurity as a white dwarf + M pair. Note that the strongest magnetic field yet discovered on a Polar is 230 MG on AR UMa (Schmidt et al. 1996).

Because SDSS J1324+0320 and SDSS J1553+5516 were selected to form the spectral template, it is no accident that these two systems lie close to the simulation path at approximately the correct field strength. However, the wide variety of spectra displayed by the examples makes it impossible to accurately model the entire picture. For example, the dominant $n = 4$ harmonic in SDSS J0837+3830 places it solidly within the low-z QSO domain of the $u-g$, $g - r$ plane, and it was targeted as such. The single weak harmonic around near 4500Å in SDSS J2048+0050 is not sufficient to move it far from the white dwarf + M star pairs. It was not targeted by the QSO algorithm, but rather as an F turnoff/subdwarf star candidate in the SEGUE extension aimed at studying the Milky Way.

It therefore appears possible that various physical and observational biases could preferentially select SDSS pre-Polar systems with magnetic field strengths in a broad interval around 60 MG. The fact that the field strength at the dominant pole of each of the six binaries discovered thus far, including the two from the Hamburg Schmidt survey, falls within just ±5% of a common value might be an artifact of small number statistics. However, we would expect to discover systems with $B \sim 50$ or 80 MG soon. If selection effects are as important as they appear to be, the total population of pre-Polars could be much larger than was postulated at the beginning of this section. Conceivably, this could strain estimates of the space density of magnetic CVs as derived from the census of Polars, but careful attention must be paid to the several Gyr that an object can hide as a detached magnetic binary with an orbit very slowly decaying by gravitational radiation.

REFERENCES

Abazajian, K., et al. 2005, AJ, 129, 1755
Baraffe, I., Chabrier, G., Allard, F., & Hauschildt, P.H. 1998, A&A, 337, 403
Baraffe, I., & Kolb, U. 2000, MNRAS, 318, 354
Beers, T.C., Allende Preito, C., Wilhelm, R., Yanny, B., & Newberg, H. 2004, PASA, 21, 207
Bergeron, P., Wesemael, F., & Beauchamp, A. 1995, PASP, 107, 1047
Beuermann, K., Baraffe, I., Kolb, U., & Weichold, M. 1998, A&A, 339, 518
Beuermann, K., & Burwitz, V. 1995, in Cape Workshop on Magnetic Cataclysmic Variables, ASP Conf. Ser., Vol. 85, ed. D.A.H. Buckley & B. Warner, (San Francisco: ASP), 99
Chanmugam, G., Barrett, P.E., Wu, K., & Courtney, M.W. 1989, ApJS, 71, 323
Cropper, M. 1988, MNRAS, 231, 597
Fan, X. 1999, AJ, 117, 2528
Ferrario, L., Wickramasinghe, D.T., & Schmidt, G. 2004, in The Astrophysics of Cataclysmic Variables and Related Objects, ASP Conf. Ser., Vol. 330, ed. J.M. Hameury & J.P. Lasota, (San Francisco: ASP), 411
Fischer, A., & Beuermann, K. 2001, A&A, 373, 211
Fukugita, M., Ichikawa, T., Gunn, J.E., Doi, M., Shimasaku, K., & Schneider, D.P. 1996, AJ, 111, 1748
Gänsicke, B.T., Hoard, D.W., Beuermann, K., Sion, E.M., & Szkody, P. 1998, A&A, 338, 933
Gänsicke, B.T., Schmidt, G.D., Jordan, S., & Szkody, P. 2001, ApJ, 555, 380
Garnavich, P.M., Szkody, P., Robb, R.M., Zurek, D.R., & Hoard, D.W. 1994, ApJ, 435, L141
Gunn, J.E., et al. 1998, AJ, 116, 3040
Gunn, J.E., & Stryker, L.L. 1983, ApJS, 52, 121
Harrison, T.E., Howell, S.B., Szkody, P., Homeier, D., Johnson, J.J., & Osborne, H.L. 2004, ApJ, 614, 947
Hawley, S., et al. 2002, AJ, 123, 3409
Henry, T.J., Kirkpatrick, J.D., & Simons, D.A. 1994, AJ, 108, 1437
Hessman, F.V., Gänsicke, B.T., & Mattei, J.A. 2000, A&A, 361, 952
Hogg, D.W., Finkbeiner, D.P., Schlegel, D.J., & Gunn, J.E. 2001, AJ, 122, 2129
Ivezic, Z., et al. 2004, AN, 325, 583
Jacoby, G.H., Hunter, D.A., & Christian, C.A. 1984, ApJS, 56, 257
Jordan, S., & Merani, N. 1995, in White Dwarfs, Proc. 9th European Workshop on White Dwarfs, ed. D. Koester & K. Werner, (Heidelberg: Springer-Verlag), p. 135
Kirkpatrick, J.D., Henry, T.J., & McCarthy, D.W. 1991, ApJS, 77, 417
Kolb, U. 2002, in The Physics of Cataclysmic Variables and Related Objects, ASP Conf. Ser., Vol. 261, ed. Gänsicke, B.T., Beuermann, K., & Reinsch, K., (San Francisco: ASP), 180
Kuijpers, J., & Pringle, J.E. 1982, A&A, 114, L4
Lamb, D.Q., & Masters, A.R. 1979, ApJ, 234, L117
Li, J.K., Wickramasinghe, D.T., & Wu, K.W. 1995, MNRAS, 276, 255
Li, J.K., Wu, K.W., & Wickramasinghe, D.T. 1994, MNRAS, 268, 61
Liebert, J., Wickramasinghe, D.T., Schmidt, G.D., Silvestri, N.M., Hawley, S.L., Szkody, P., Ferrario, L., Webbink, R.F., Oswalt, T.D., Smith, J. Allyn, & Lemagie, M.P. 2005, AJ, 129, 2376
Lupton, R.H., Gunn, J.E., Szalay, A.S. 1999, AJ, 118, 1406
Lupton, R.H., Gunn, J.E., Ivezic, Z., Knapp, G.R., Kent, S.M., & Yasuda, N. 2001, in Astronomical Data Analysis Software & Systems X, ASP Conf. Ser., Vol. 238, ed F.R. Harnden, Jr., F.A. Primini, & H.E. Payne, (San Francisco: ASP), 269
Massey, P., Strobel, K., Barnes, J.V., & Anderson, E. 1988, ApJ, 328, 315

Mauche, C. 1999, in Annapolis Workshop on Magnetic Cataclysmic Variables, ASP Conf. Ser., Vol. 157, ed. C. Hellier & K. Mukai, (San Francisco: ASP), 157
Meggitt, S.M.A., & Wickramasinghe, D.T. 1982, MNRAS, 198, 71
Merani, N., Main, J., & Wunner, G. 1995, A&A, 298, 193
Pier, J.R., Munn, J.A., Hindsley, R.B., Hennessy, G.S., Kent, S.M., Lupton, R.H., & Ivezic, Z. 2003, AJ, 125, 1559
Andronov, N., Pinsonneault, M.H., & Sills, A. 2003, ApJ, 582, 358
Ramsay, G., Cropper, M., Wu, K., Mason, K.O., Córdova, F.A., & Priedhorsky, W. 2004, MNRAS, 350, 1373
Reimers, D., & Hagen, H.-J. 2000, A&A, 358, L45
Reimers, D., Hagen, H.-J., & Hopp, U. 1999, A&A, 343, 157
Richards, G.T., et al. 2002, AJ, 123, 2945
Ritter H., & Kolb U. 2003, A&A, 404, 301
Rousseau, Th., Fischer, A., Beuermann, K., & Woelk, U. 1996, A&A, 310, 526
Schmidt, G. 2004, in The Astrophysics of Cataclysmic Variables and Related Objects, ASP Conf. Ser., Vol. 330, ed. J.M. Hameury & J.P. Lasota, (San Francisco: ASP), 125
Schmidt, G.D., Stockman, H.S., & Grandi, S.A. 1986, ApJ, 300, 804
Schmidt, G.D., Stockman, H.S., & Smith, P.S. 1992, ApJ, 398, L57
Schmidt, G.D., Szkody, P., Smith, P.S., Silber, A., Tovmassian, G., Hoard, D.W., Gänsicke, B.T., & de Martino, D. 1996, ApJ, 473, 483
Schmidt, G.D., West, S.C., Liebert, J., Green, R.F., & Stockman, H.S. 1986, ApJ, 309, 218
Schwarz, R., Schwope, A.D., & Staude, A. 2001, A&A, 374, 189
Schwope, A.D., Brunner, H., Hambaryan, V., Schwarz, R., Staude, A., Szokoly, G., & Hagen, H.-J. 2002, in The Physics of Cataclysmic Variables and Related Objects, ASP Conf. Ser., Vol. 261, ed. Gänsicke, B.T., Beuermann, K., & Reinsch, K., (San Francisco: ASP), 102
Silvestri, N.M., Lemagie, M.P., Hawley, S.L., Schmidt, G.D., Szkody, P., Liebert, J., & Wolfe, M.A. 2005, AJ, in preparation
Sion, E.M. 1999, PASP, 111, 532
Smith, J.A., et al. 2002, AJ, 123, 2121
Stoughton, C., et al. 2002, AJ, 123, 485
Szkody, P., et al. 2003, ApJ, 583, 902 (S03)
Szkody, P., et al. 2005, AJ, 129, 2386
Szkody, P., Homer, L., Chen, B., Henden, A., Schmidt, G., Anderson, S., Hoard, D., Voges, W., & Brinkmann, J. 2004, AJ, 128, 2443 (S04)
Townsley, D.M., & Bildsten, L. 2002, in The Physics of Cataclysmic Variables and Related Objects, ASP Conf. Ser., Vol. 261, ed. Gänsicke, B.T., Beuermann, K., & Reinsch, K., (San Francisco: ASP), 31
———.2004, ApJ, 600, 390
Vennes, S., Szkody, P., Sion, E.M., & Long, K.S. 1995, ApJ, 445, 921
Verbunt, F., & Zwaan, C. 1981, A&A, 100, L7
Wargelin, B.J., & Drake, J.J. 2001, ApJ, 546, L57
Warner, B. 1995, Cataclysmic Variable Stars (Cambridge: Cambridge Univ. Press)
Webbink, R.F., & Wickramasinghe, D.T. 2004, in The Astrophysics of Cataclysmic Variables and Related Objects, ASP Conf. Ser., Vol. 330, ed. J.M. Hameury & J.P. Lasota, (San Francisco: ASP), 137
Webbink, R.F., & Wickramasinghe, D.T. 2002, MNRAS, 335, 1
Wheatley, P.J., & Ramsay, G. 1998, in ASP Conf. Ser., Vol. 137, Wild Stars in the Old West, ed. S. Howell, E. Kuulkers, & C. Woodward (San Francisco: ASP), 446
Wickramasinghe, D.T., & Ferrario, L. 2000, PASP, 112, 873
Woelk, U., & Beuermann, K. 1992, A&A, 256, 498
———.1996, A&A, 306, 232
York, D.G., et al. 2000, AJ, 120, 1579

TABLE 1
LOG OF OBSERVATIONS

Object (SDSS+)	UT Date (yyyymmdd)	Telescope	Type	Duration (h:mm)	Comments
J083751.00+383012.5	20020212	SDSS 2.5 m	Spectroscopy	0:45	
	20040424	MMT	Cir. spectropol.	1:13	
	20040513	MMT	Cir. spectropol.	1:27	
	20040921	MMT	Cir. spectropol.	0:35	
	20041130	MDM 2.4 m	CCD imaging	2:56	poor seeing
	20041201	MDM 2.4 m	CCD imaging	4:44	poor seeing
	20050316	Bok 2.3 m	Cir. spectropol.	0:30	
J132411.57+032050.5	20030529	MMT	Cir. spectropol.	2:28	
	20040216	MMT	Cir. spectropol.	2:59	
J155331.12+551614.5	20020318	Bok 2.3 m	Cir. spectropol.	3:27	clouds at end
	20020508	Bok 2.3 m	Cir. spectropol.	4:16	
	20040216	MMT	Cir. spectropol.	0:18	
J204827.91+005008.9	20040824	SDSS 2.5 m	Spectroscopy	1:33	
	20040916	Bok 2.3 m	Cir. spectropol.	1:12	cirrus
	20041004	APO 3.5 m	Spectroscopy	4:18	

TABLE 2
SDSS PHOTOMETRY

Object	g	$u-g$	$g-r$	$r-i$	$i-z$
SDSS J083751.00+383012.5	19.14	+0.01	+0.03	+0.49	+0.70
SDSS J204827.91+005008.9	19.38	+0.56	+0.70	+1.08	+0.68

TABLE 3
LOW ACCRETION-RATE MAGNETIC BINARIES

Object	Period (h)	Mag.[a]	B[b] (MG)	$\dot{M}$ ($M_\odot$ yr^{-1})	D (pc)	Sp. Type (secondary)	Ref.
SDSS J1324+0320	2.60	22.1	64	$\sim 1 \times 10^{-13}$	450	M6	5,6,7
WX LMi (HS 1023+3900)	2.78	18.0	60(68)	$< 3 \times 10^{-13}$	140	M4.5	1,3,4
SDSS J0837+3830	3.18 or 3.65	19.1	65(??)	$\sim 2 \times 10^{-13}$	330	M5	7
HS 0922+1333	4.07	19	66(81:)	$\sim 3 \times 10^{-13}$	190	M3.5	2,4
SDSS J2048+0050	4.2	19.7	62:	$\sim 5 \times 10^{-14}$	260	M3	7
SDSS J1553+5516	4.39	18.5	60	6×10^{-14}	130	M5	5,6,7

[a]g for SDSS objects; B for HS objects.

[b]Parentheses denote secondary pole.

References. — (1) Reimers et al. (1999); (2) Reimers & Hagen (2000); (3) Schwarz et al. (2001); (4) Schwope et al. (2002); (5) Szkody et al. (2003); (6) Szkody et al. (2004); (7) This paper.
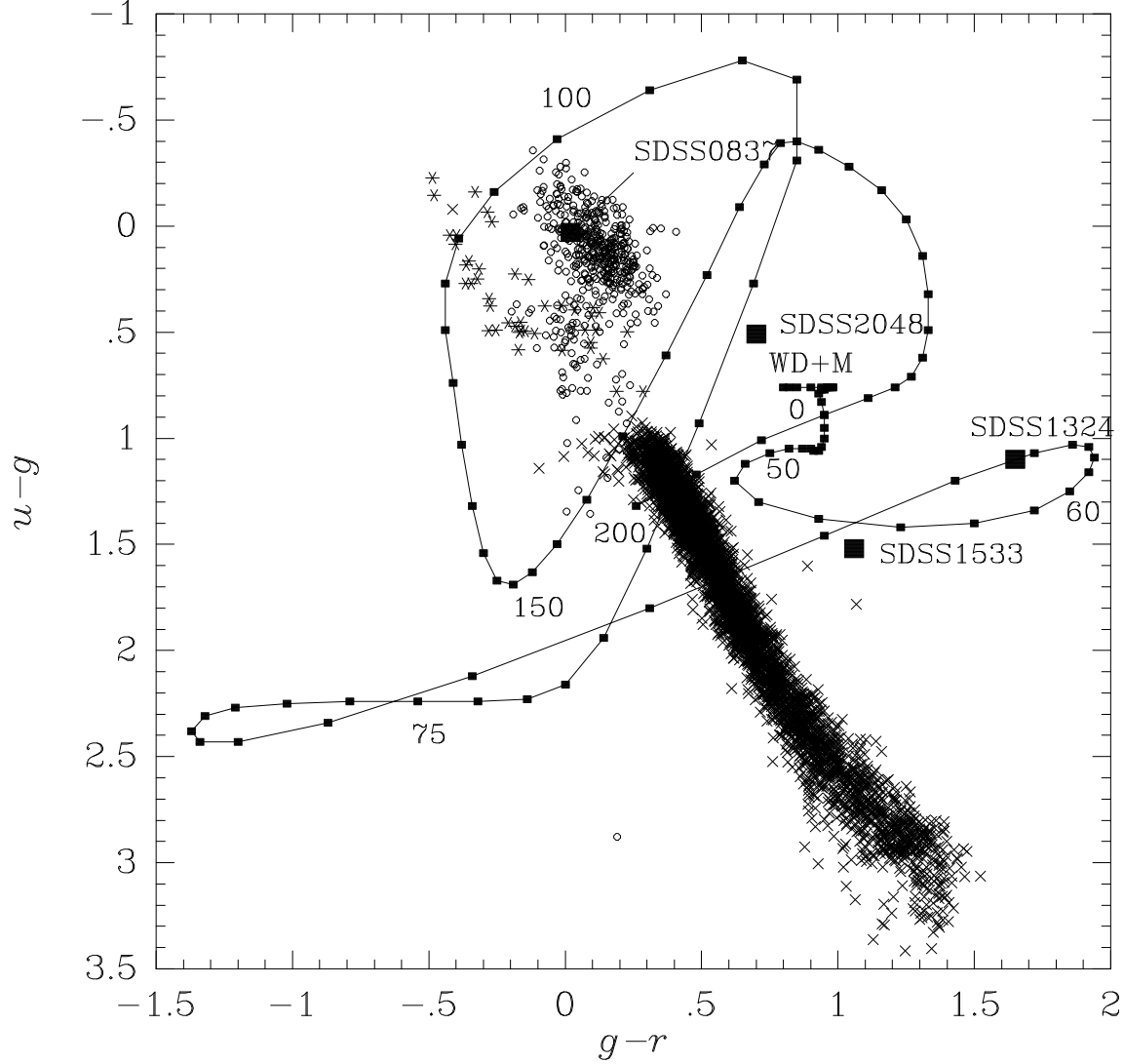
FIG. 1.— Locations of the four SDSS low-$\dot{m}$ magnetic accretion binaries in the $u - g$, $g - r$ color-color plane. Also shown are disk stars *(crosses)*, white dwarfs *(stars)*, and QSOs *(circles)*, taken from the North Galactic Pole SDSS color simulations of Fan (1999). The approximate location of white dwarf + M star pairs is indicated, but the QSO targeting algorithm actually defines this excluded region according to $g - r$, $r - i$ colors. Only objects with $g < 21$ are shown, and measured color bands differ slightly from those used in the Fan simulations, but the data suffice for illustrative purposes. The serpentine path depicts the track of a model low-$\dot{m}$ magnetic system with field strength varying from $0 - 200$ MG, as marked and discussed in §8.
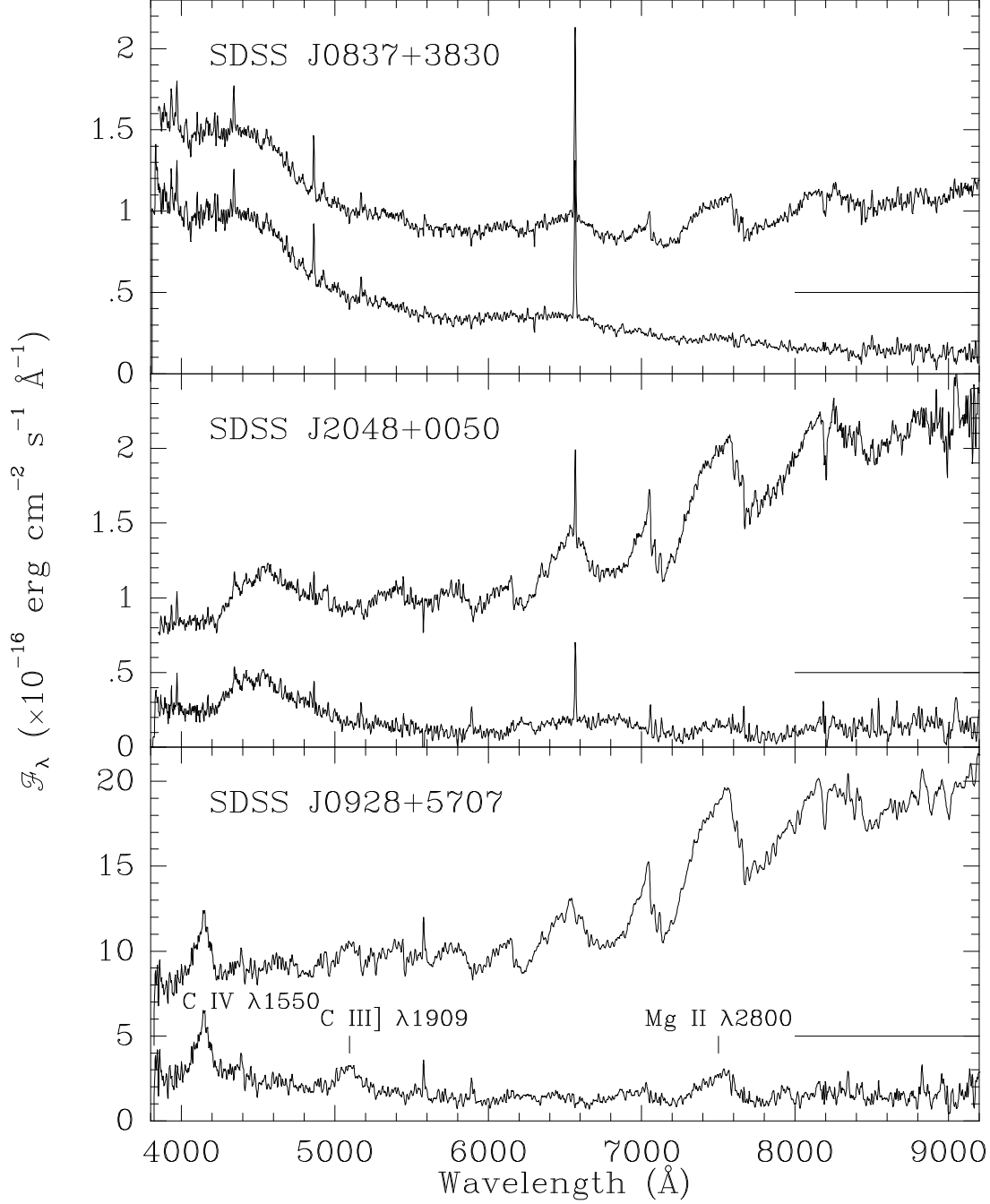
FIG. 2.— *(Top and middle, bold)*: Observed SDSS spectra of the two new magnetic accretion binaries. Each exhibits a clear hump in the blue that is found to be strongly polarized, plus an M-star continuum at longer wavelengths. Spectra are displaced upward for clarity, with the zero-point of the flux scale indicated at right. *(Narrow)*: Spectra after subtraction of the best-fitting late-type main-sequence star. See text for details. *(Bottom, bold)*: The spectrum of SDSS J0928+5707 appears qualitatively similar to those in the upper panels, but it is unpolarized. *(Narrow)*: Subtraction of an M3 V spectrum reveals that the object is a superposition with a QSO at $z = 1.67$. Comparison of the observed spectra of SDSS J0837+3830 and SDSS J2048+0050 with the examples from Szkody et al. (2003) attest to the wide range in spectral properties displayed by the class.
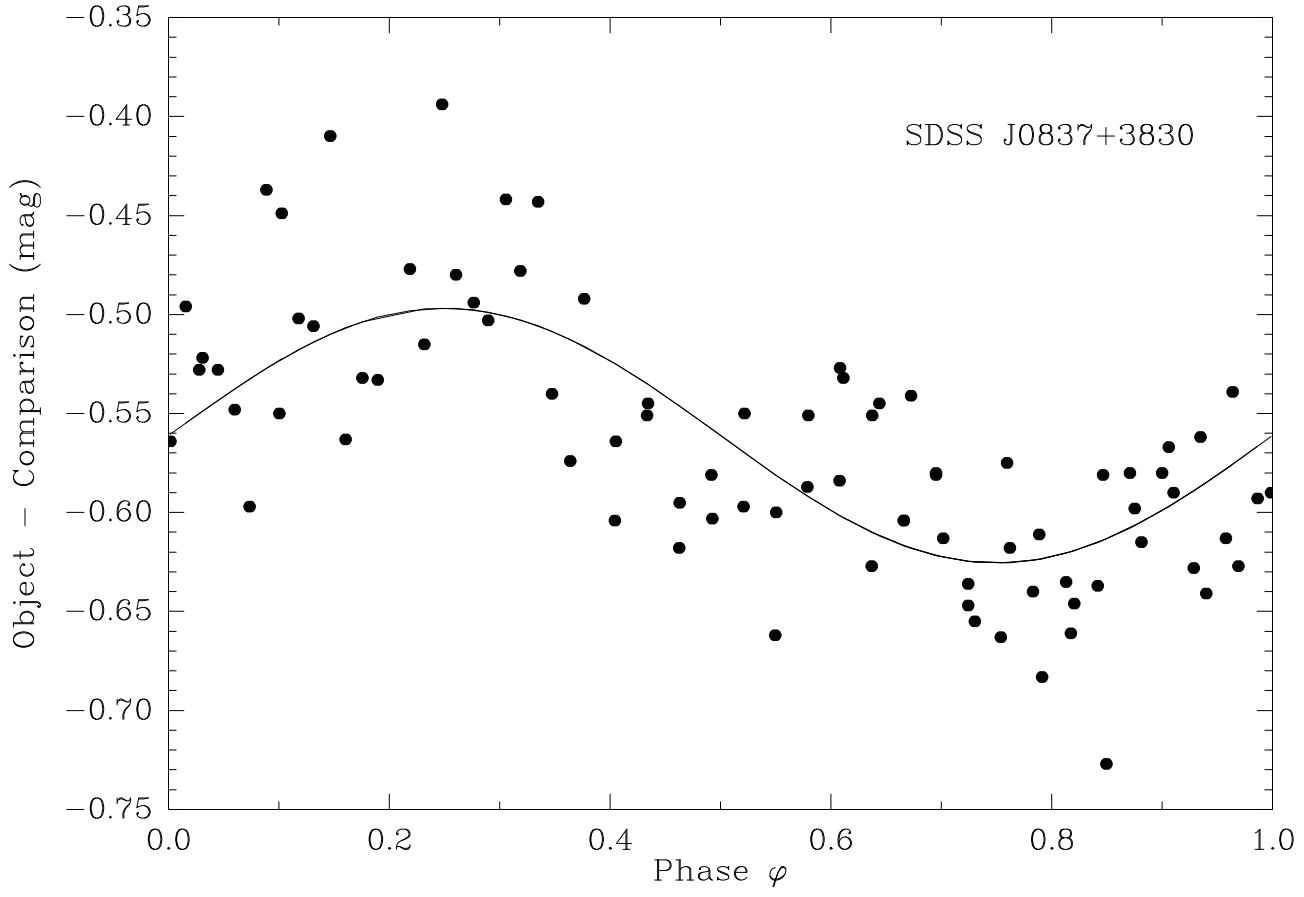
FIG. 3.— Two consecutive nights of CCD photometry of SDSS J0837+3830 phased on a period of 3.18 hr. The least-squares fit sine wave semiamplitude is 0.06 mag. Scatter is attributable to poor seeing during the observations.
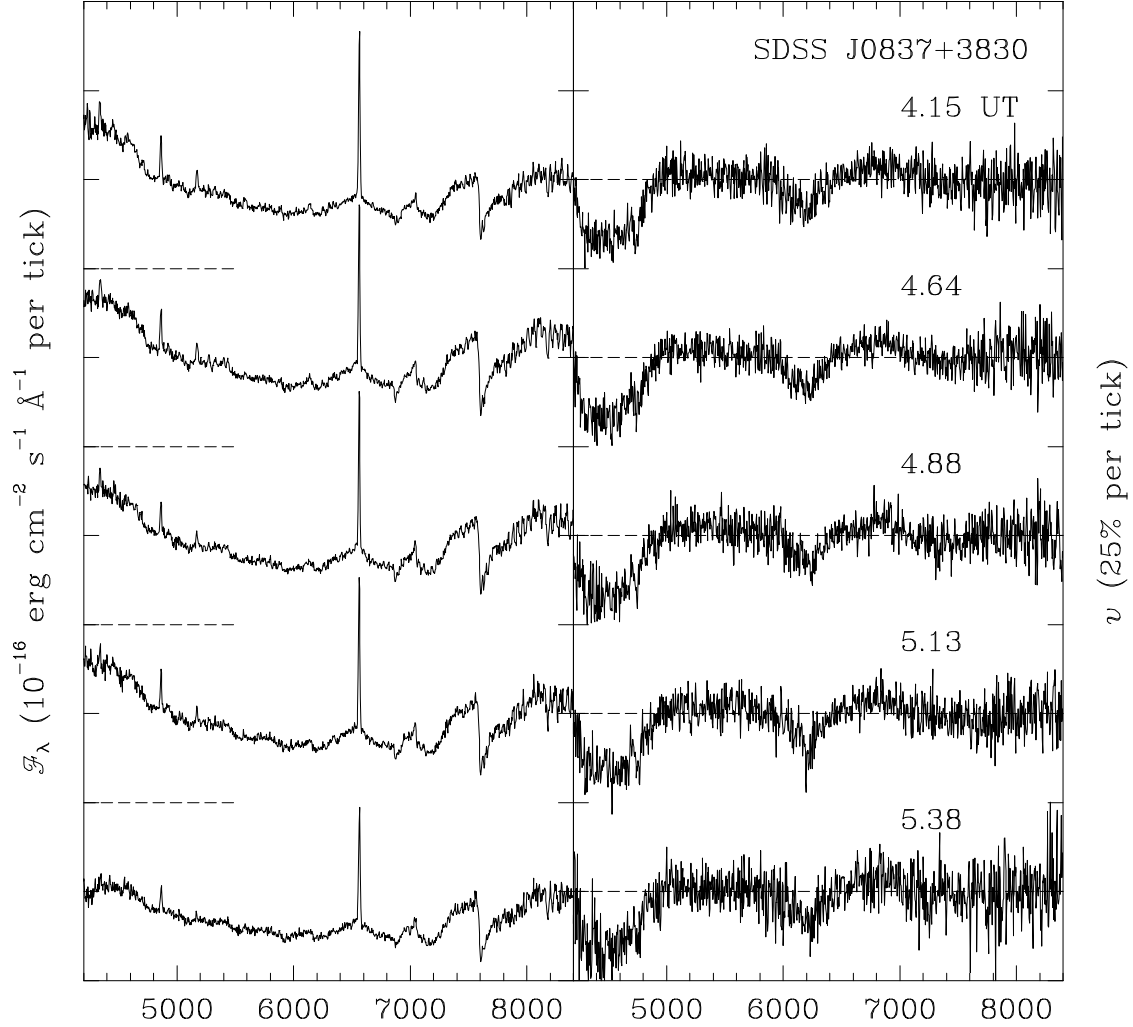
FIG. 4.— Spectral flux *(left)* and circular polarization *(right)* for SDSS J0837+3830 on 2004 May 13. Sequences cover 1.23 hr, or nearly 40% of the orbital period, with the mid-UT of each spectrum indicated in the right panel. The only convincing change through the series is a decrease in the emission-line strength, likely due to our varying view of the inner hemisphere of the secondary star. Note the distorted appearance in polarization of the harmonic at 6200Å and the weak positive circular polarization between harmonics, indicating that accretion occurs onto both magnetic poles.
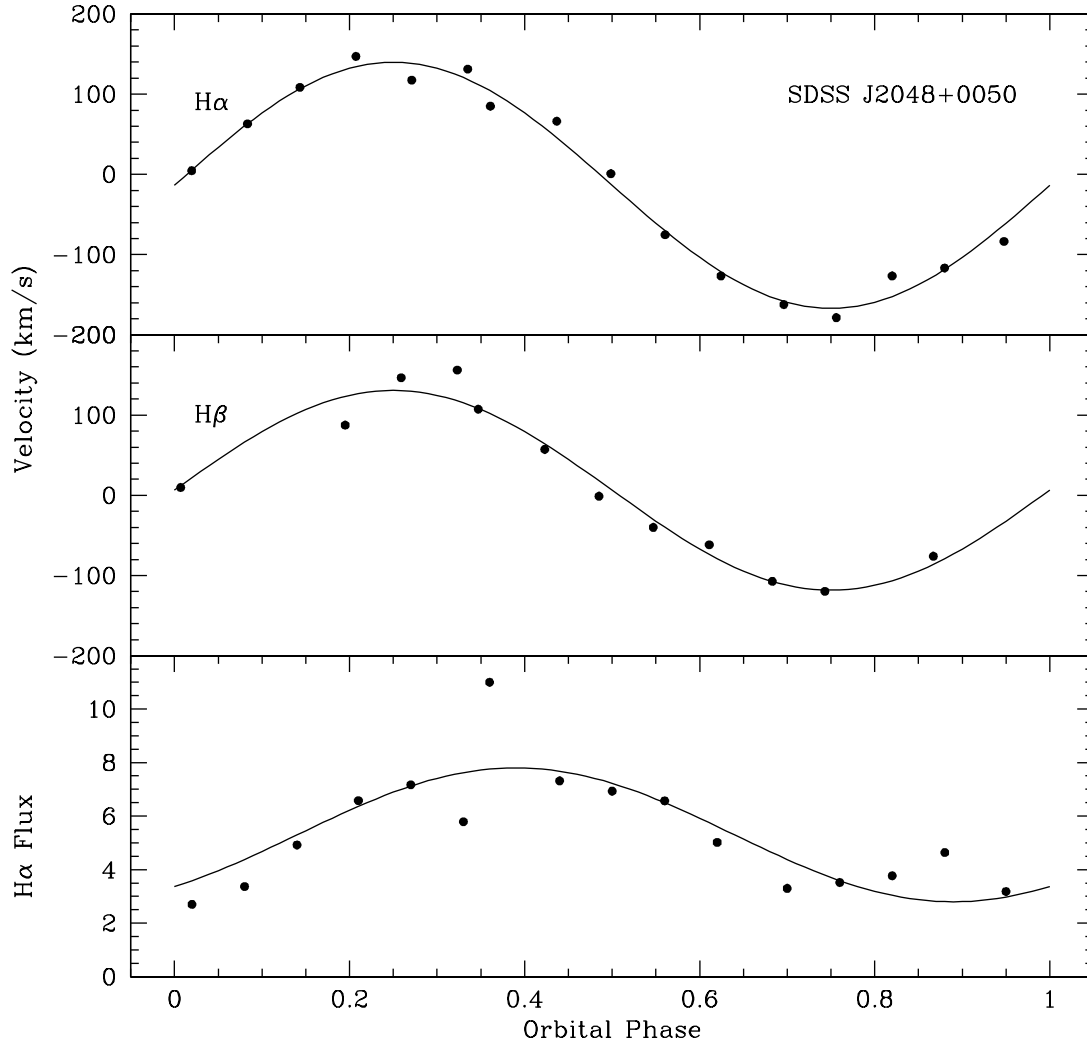
FIG. 5.— Emission-line velocities and Hα flux (in units of 10^{-16} erg cm^{-2} s^{-1}) for SDSS J2048+0050, phased on a period of 4.2 hr, with $\varphi = 0$ defined by the positive zero-crossing of radial velocity.
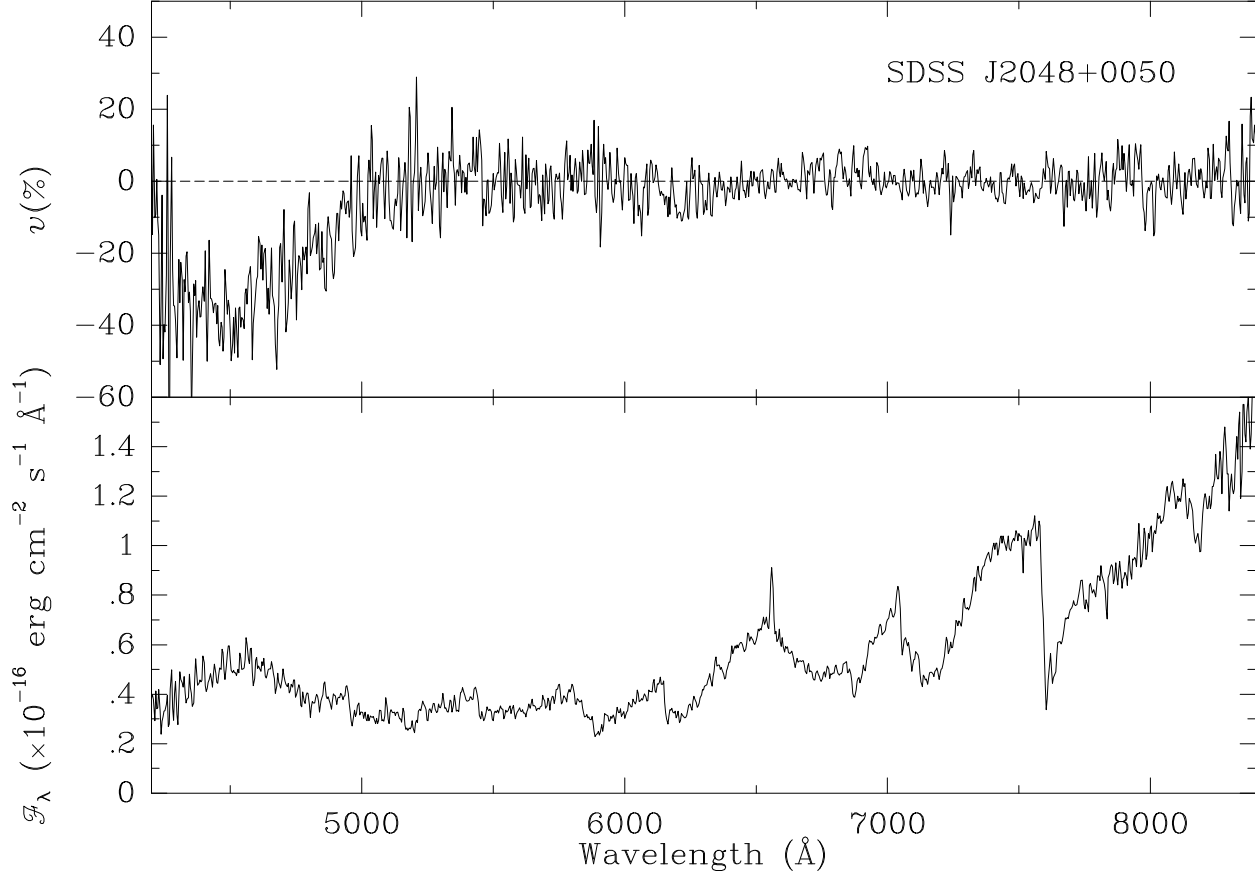
FIG. 6.— Spectral flux *(bottom)* and circular polarization *(top)* for SDSS J2048+0050 on 2004 Sep. 16. In addition to the strongly-polarized cyclotron hump around λ4550, a very weak harmonic may be present near 6200Å. This would indicate a magnetic field strength of ∼62 MG. The data represent slightly more than 1 hr of exposure, or about one-quarter of the period. The measured polarization in the 4550Å harmonic, coupled with the strength of the hump in total flux, implies that the cyclotron emission in this feature is essentially 100% circularly polarized.
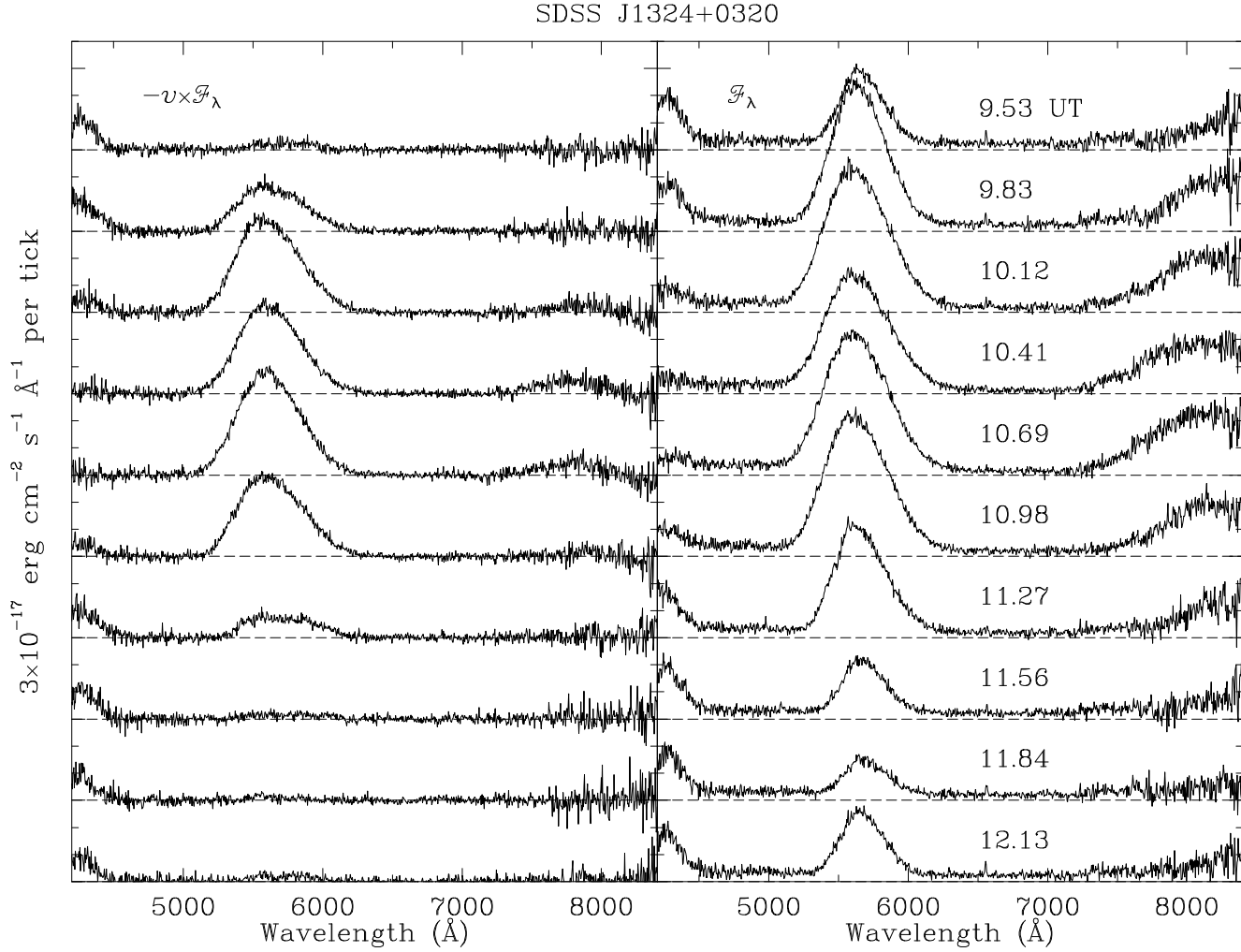
FIG. 7.— Spectrum of circularly polarized flux, $-v \times F_\lambda$ *(left)*, and total flux F_λ *(right)*, *vs.* UT as marked, covering a full 2.6 hr cycle of SDSS J1324+0320 on 2004 Feb. 16. The total flux spectrum is shown after the subtraction of an M6 V stellar template, the spectral type judged to best match the observed stellar features. Note that the polarized flux has been negated to facilitate comparison with the total flux spectrum.
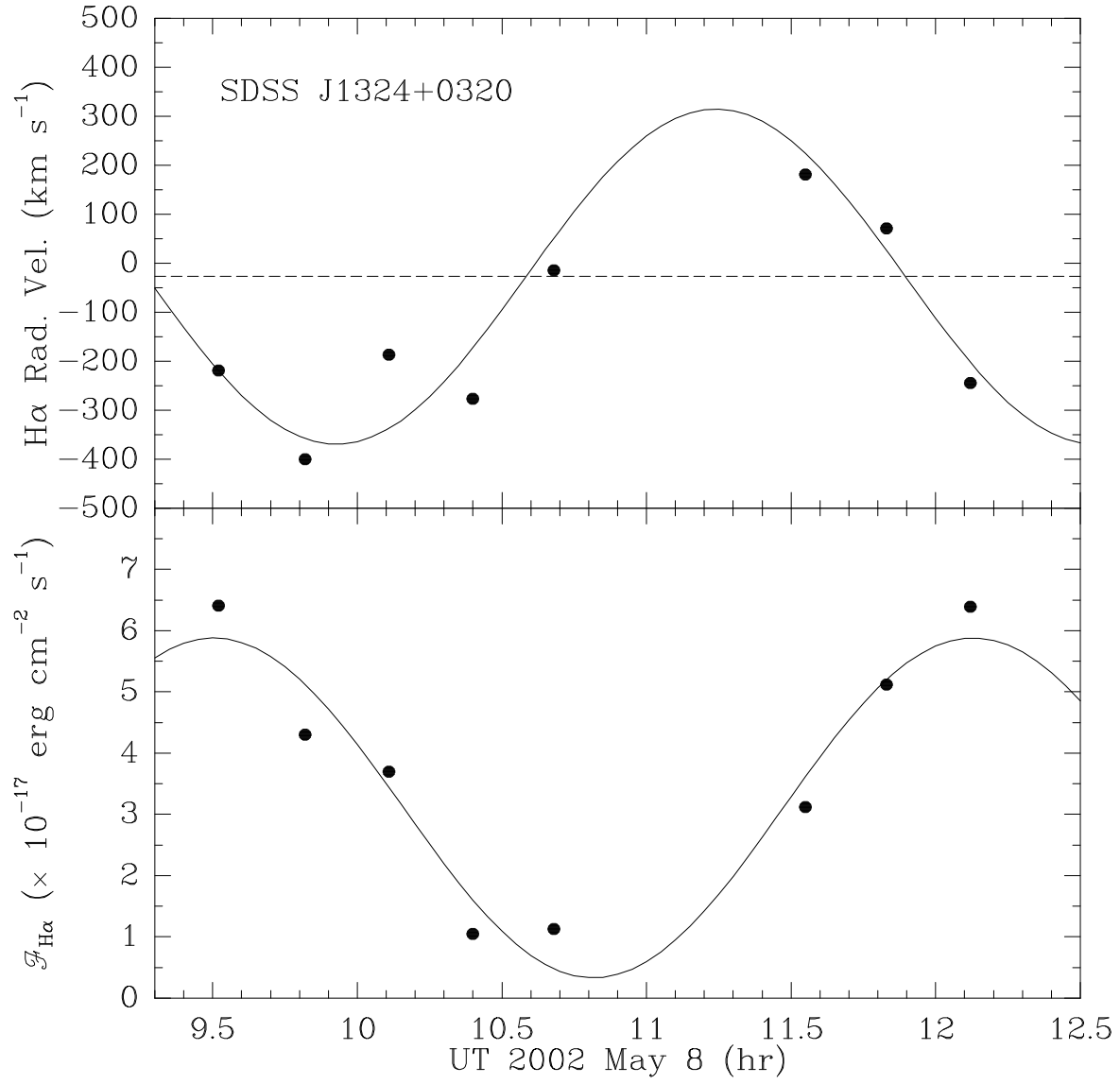
Fig. 8.— Radial velocity *(top)* and flux *(bottom)* of the weak, narrow Hα emission line of SDSS J1324+0320 *vs.* UT from the data of Figure 7. The best-fit period (shown) has a value of 2.62 ± 0.24 hr. Note that the minimum Hα flux and positive zero-crossing of radial velocity coincide with the peak in flux of the $n = 3$ cyclotron harmonic in Figure 6, indicating that the spin and orbital periods are essentially locked and that the emission line arises on the inner hemisphere of the secondary star.
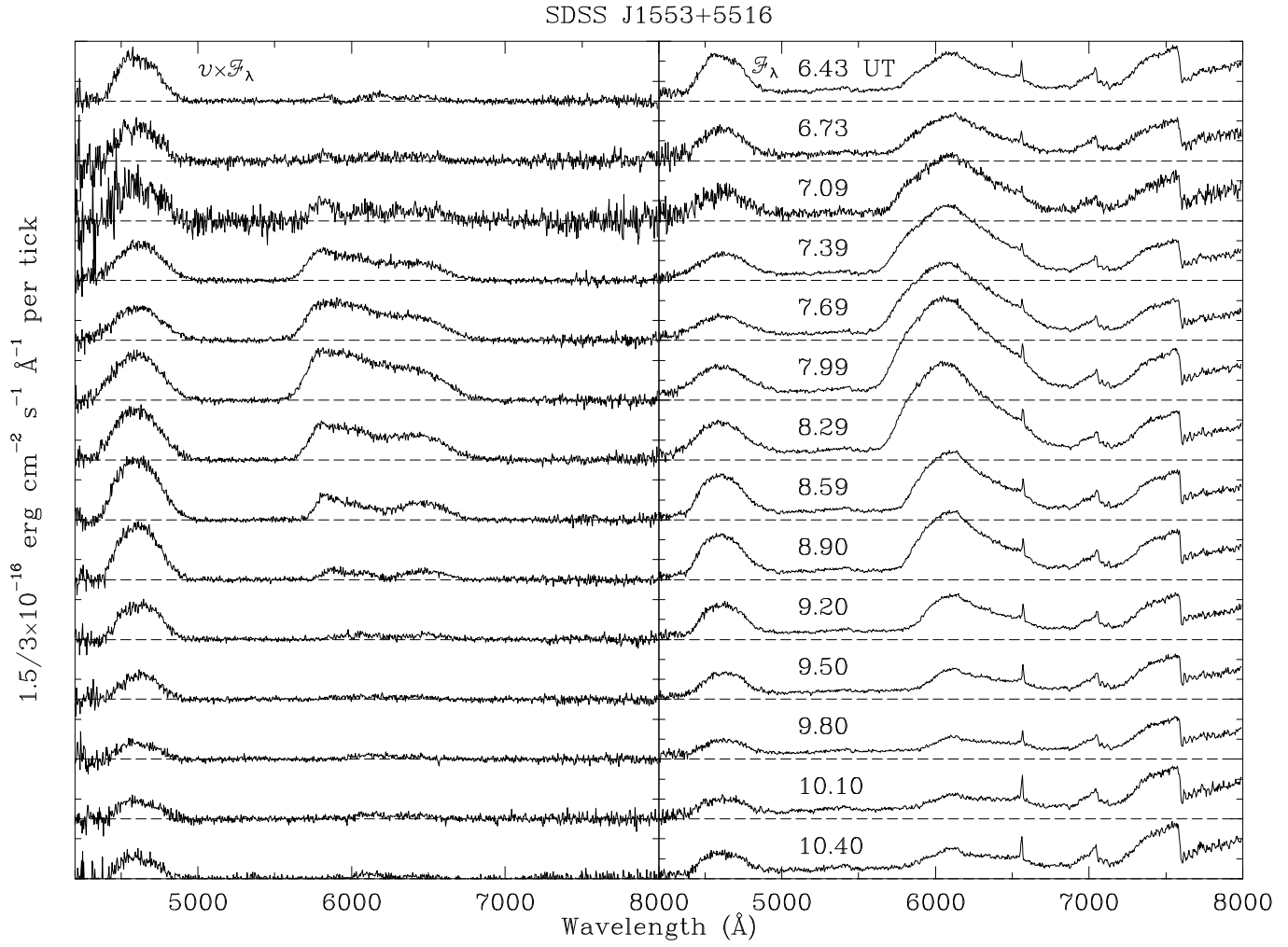
SDSS J1553+5516

FIG. 9.— Spectrum of circularly polarized flux, $v \times F_\lambda$ *(left)*, and total flux F_λ *(right)*, vs. UT as marked, covering nearly a complete cycle of SDSS J1553+5516 on 2002 May 8. Scaling of the ordinate differs by a factor 2 between the two panels, as indicated.
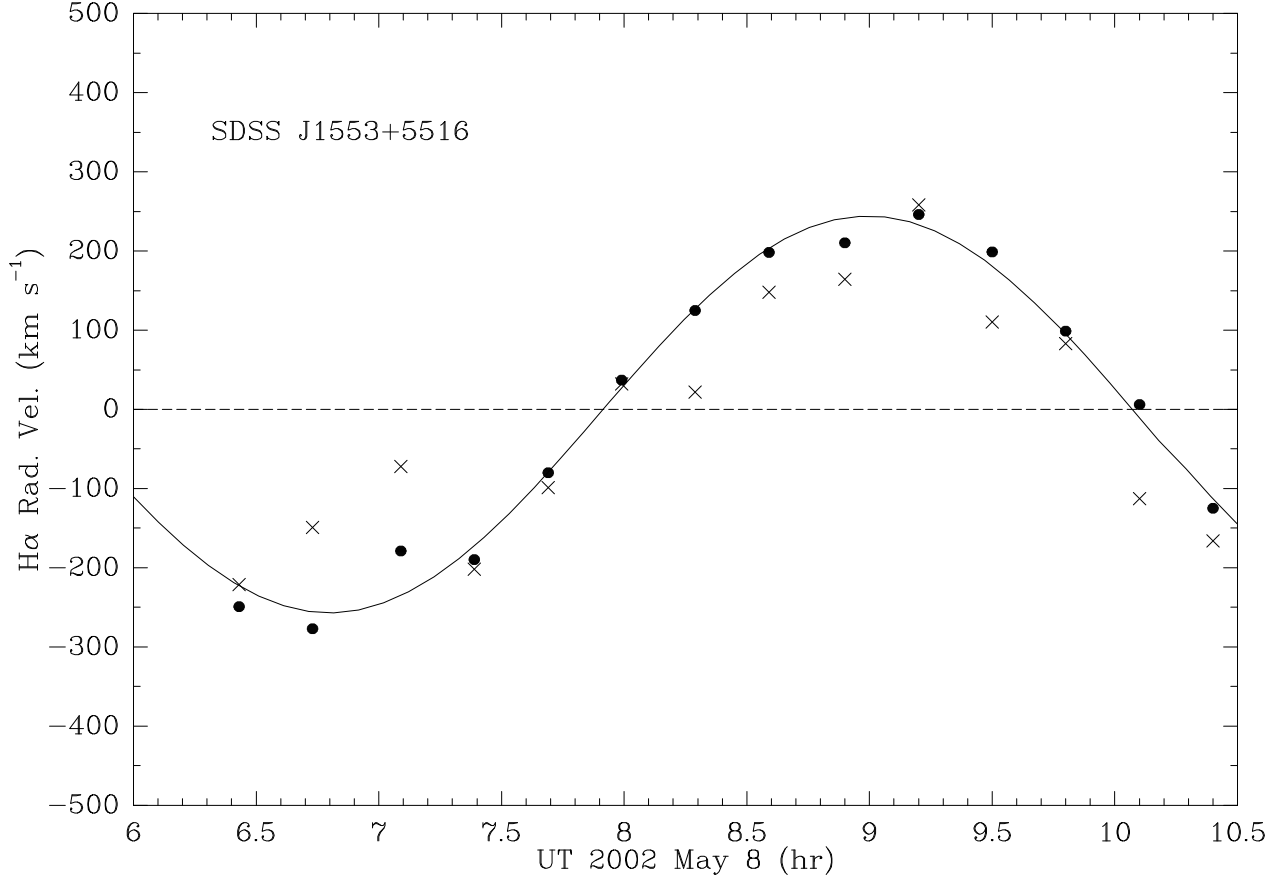
Fɪɢ. 10.— Radial velocity of the Hα emission line *(circles)* and 7050Å TiO bandhead *(crosses)* of SDSS J1553+5516 *vs.* UT from the data of Figure 9. The common phasing and semiamplitude (250 km s^{-1}) of the two features confirm that the emission lines originate on the secondary star.
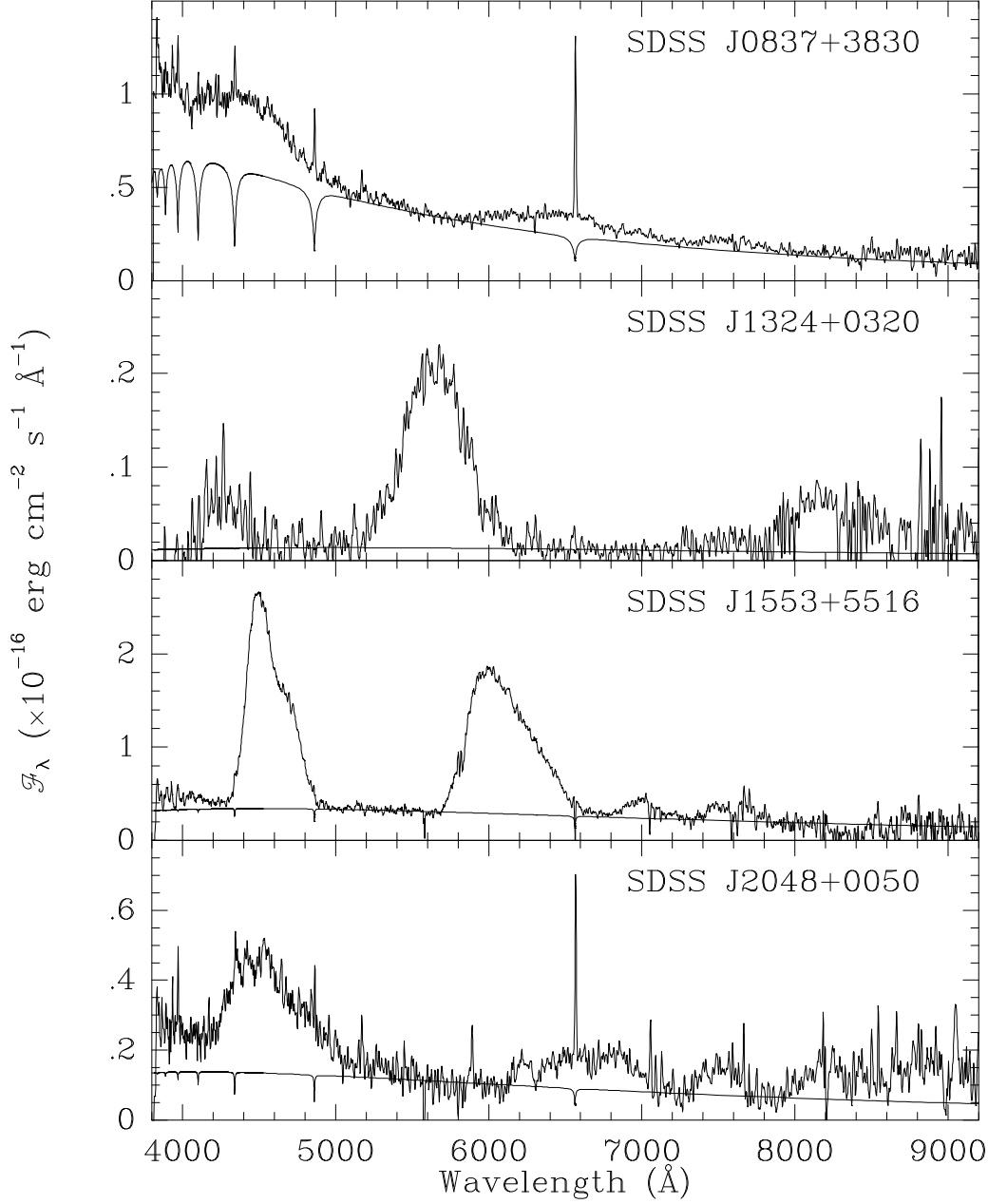
Fig. 11.— Secondary-subtracted survey spectra of the four SDSS low-$\dot{m}$ systems *(bold)*, with the energy distributions of white dwarf photospheres plotted below *(narrow)*, where the stellar temperatures have been computed according to the measured spectral flux between cyclotron harmonics in the $5000 - 5600$Å interval. The implied white dwarfs are unusually cool for accretion binaries, with $T_{\rm eff}$ ranging from 5,500 K for SDSS—J1324+0320 to 9,500 K for SDSS J0837+3830. Note, however, that the stellar continuum falls short of the observed flux near 4000Å in at least SDSS J1553+5516 and SDSS J2048+0050, suggesting the presence of an irradiated hot spot surrounding the pole(s).

APPENDIX

DISTANCE ESTIMATION FROM NEW CALIBRATED M DWARF SPECTRA

While the specific accretion rate (e.g., gm cm^{-2} s^{-1}) in a magnetic binary can be determined from spectroscopic analysis and/or an X-ray to optical flux ratio, a total mass-transfer rate requires distance information. Often, the only clue to this comes from the spectrum of a stellar component coupled with an assumption as to the structural state of the star. Disregarding indications to the contrary at certain orbital periods (Beuermann et al. 1998 and references therein), the ZAMS relation is often assumed for secondaries in CVs, and in the absence of strong radiative heating, spectral types and luminosities appropriate to main-sequence stars are also taken to apply. In the case of chronically very low accretion-rate magnetic binaries, where mass transfer does not occur through Roche-lobe overflow and there is good reason to believe that contact with the Roche surface has never been established, mass loss has not had the opportunity to affect stellar structure, and the assumption of main-sequence properties are especially secure. Unfortunately, even though spectral types of late-type dwarfs are generally based on optical line and band ratios (Kirkpatrick et al. 1991), absolute energy outputs of the stars are generally given in broad-band optical and/or infrared absolute magnitudes (e.g., Henry et al. 1994; Baraffe et al. 1998; Hawley et al. 2002). The use of these to estimate distances to new objects solely from optical spectra not only involves computational steps, but the process can be problematic for binaries where additional emission components are present (primary star, accretion disk, cyclotron radiation). Moreover, available spectral atlases (e.g., Gunn & Stryker 1983; Jacoby et al. 1984) often do not extend sufficiently far into the red to enable comparison, or were taken with rather narrow entrance slits or under non-photometric conditions, so absolute flux calibrations cannot be trusted. It therefore seemed appropriate to acquire a new sequence of M dwarf spectra for the express purpose of establishing monochromatic flux trends suitable for distance estimation to short-period binaries.

Fourteen stars with spectral types M0 to M6.5 V were chosen for observation from the RECONS[18] list of the 100 nearest stars. The stars observed are: G099−049, GJ 205, GJ 229A, GJ 273, GJ 285, GJ 299, GJ 338A, GJ 406, GJ 408, GJ 411, GJ 412A, GJ 412B, GJ 1111, and GJ 1116A. Distances are known from parallax measurements to an uncertainty of 5% for all cases, and to <2% in the vast majority. The entire list was observed in a 2 hr period of steady, photometric conditions with 1″.5 FWHM seeing with the 2.3 m Bok telescope using the spectropolarimeter operating as a simple spectrograph. The region $4200 - 8200$Å was available in a single grating setting at a resolution of ∼15Å. An entrance aperture of width 5″ width ensured low slit losses, and absolute spectral response functions were based on observations of 3 standard stars calibrated by Massey et al. (1988), measured both before and after the program stars. Atmospheric extinction corrections used mean coefficients for Kitt Peak, but in the interests of efficiency the terrestrial O_2 band features in the red were not removed. This would have required the observation of an additional star with a featureless spectrum near each of the program targets.

Spectra that sample the range in spectral type are shown in Figure A1. To facilitate their use in estimating distances, five narrow bands were selected in regions where the flux is not changing strongly with wavelength and away from deep molecular bands, chromospheric emission lines, and terrestrial absorption features. For the band redward of 7000Å, an additional requirement was that the bandwidth be broader than the fringing period caused by optical interference in the CCD. Mean spectral fluxes (in units of erg cm^{-2} s^{-1} Å^{-1}) in these bands were computed for each star and the values adjusted to a common distance of 10 pc. The results are displayed in Figure A2 for all 14 stars, using spectral types provided on the RECONS web page. Also shown are least-squares fits to relations of the form

$$\log(F_\lambda) = A + B \cdot S^C \tag{A1}$$

where S is the M subtype. For all bands, it was found that a value of $C = 1.6$ adequately reflects the curvature in the relations, and least-squares values for the fitting coefficients A and B are given in Table A1.

The mean dispersion around the fits amounts to slightly less than 50% in flux, equivalent to a distance uncertainty of somewhat more than 20%. This is considerably greater than the distance uncertainty in any single star, and is far too large to be explained by flux calibration errors in the calibration spectra. Instead, the dispersion is likely attributable to differences in spectral classification (typically equivalent to an uncertainty of ∼0.5 subtype), plus possibly real variations among the stars within a subtype, and reflects the limitations of the technique.

[18] Research Consortium on Nearby Stars; http://www.chara.gsu.edu/RECONS.

TABLE A1
FITTING COEFFICIENTS
FOR MONOCHROMATIC
FLUX RELATIONS

Band	A^a	B^a
$4700 - 4740$	-12.23	-0.179
$5100 - 5150$	-12.29	-0.165
$6100 - 6140$	-11.97	-0.174
$6760 - 6840$	-12.04	-0.159
$7450 - 7500$	-11.85	-0.122

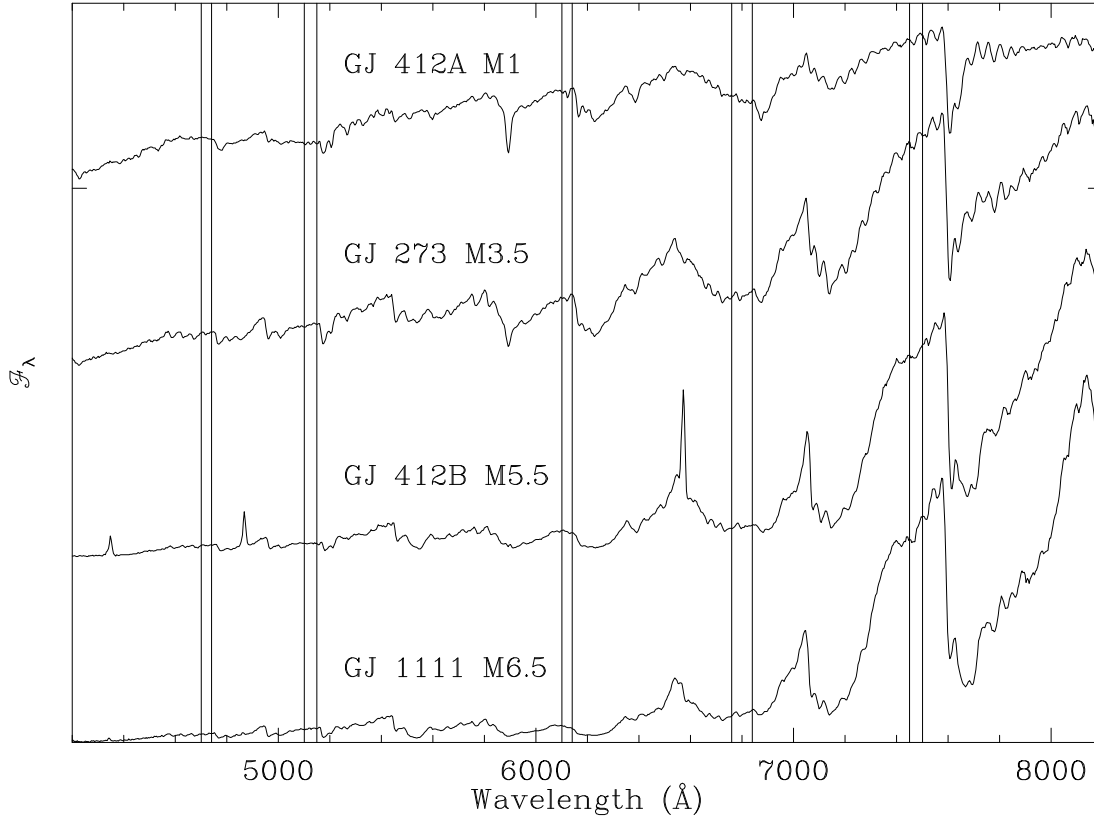$^a F_\lambda$ in units of erg cm^{-2} s^{-1}
Å^{-1}, for a distance of 10 pc.

FIG. A1.— Sample M dwarf spectra obtained with a resolution of ∼15Å to calibrate monochromatic absolute flux-spectral type relations. Narrow bands defined for the analysis are marked.
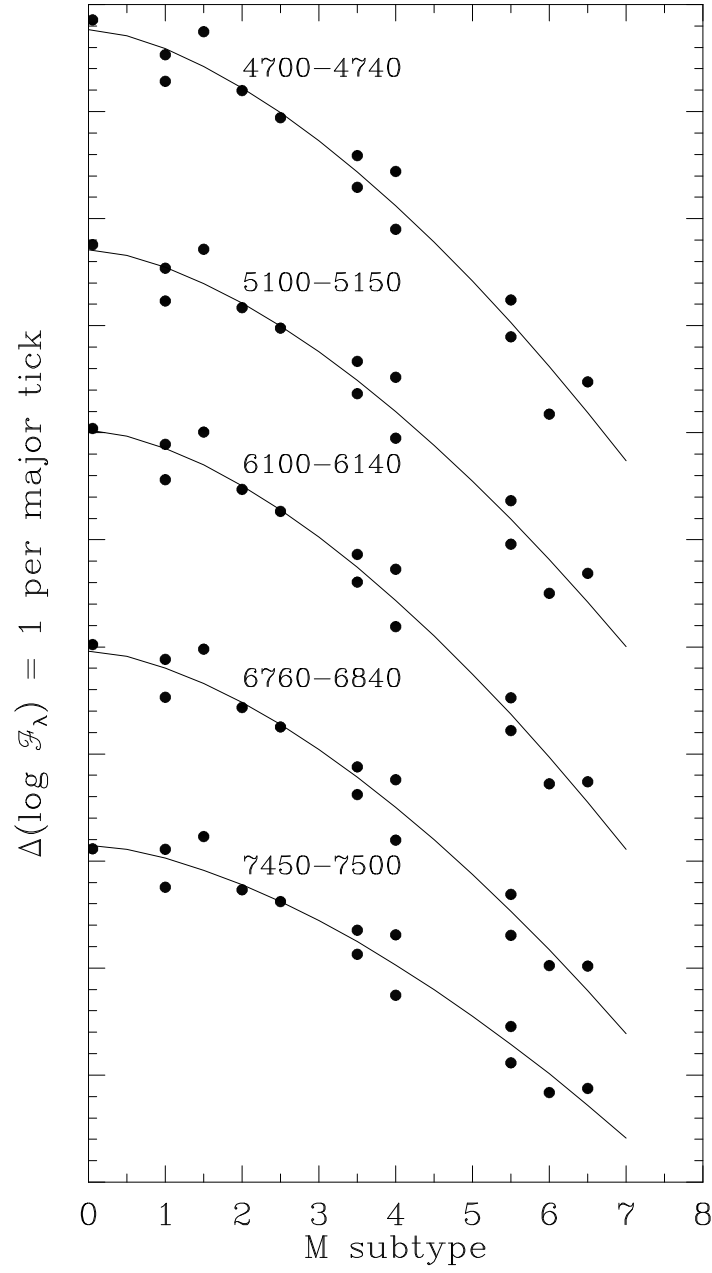
FIG. A2.— Dependence of spectral flux in the narrow bands of Figure A1 - adjusted to a common distance of 10 pc - on M subtype, with a displacement of 2 dex between successive relations. Equations describing the fits are provided in the text.